Effect of HPO42– and brushite on gypsum reactivity and implications for utilization of phosphogypsum in plaster production

Hajar Bellefqih, Véronique Bourgier, Essaid Bilal, Delia-Georgeta Dumitraş, Stefan Marincea, Hamid Mazouz, Nils Haneklaus

Journal of Cleaner Production 451 (2024) 142013

Contents lists available at ScienceDirect

Journal of Cleaner Production

journal homepage: www.elsevier.com/locate/jclepro

Effect of HPO_4^{2-} and brushite on gypsum reactivity and implications for utilization of phosphogypsum in plaster production

Hajar Bellefqih [a], Véronique Bourgier [a], Essaid Bilal [a], Delia-Georgeta Dumitraş [b], Ştefan Marincea [b], Hamid Mazouz [c], Nils Haneklaus [d,e,*]

[a] Ecole Nationale Supérieure des Mines de Saint Etienne, CNRS UMR, EVS, 5600, F42023, Saint Etienne, France
[b] Geological Institute of Romania, Caransebeş Street, No. 1, Sector 1, 012271, Bucharest, Romania
[c] Division of Research and Innovation (DRI), Mohammed VI Polytechnic University (UM6P), Ben Guerir, 43150, Morocco
[d] Technische Universität Bergakademie Freiberg, Leipziger Straße 29, Freiberg, Germany
[e] Universität für Weiterbildung Krems, Td-Lab Sustainable Mineral Resources, Krems, Austria

ARTICLE INFO

Handling Editor: Jian Zuo

Keywords:
Phosphogypsum
Gypsum
Phosphorus impurities
Brushite
Ardealite
Monetite
Syncrystallized HPO_4^{2-} ions

ABSTRACT

The implementation of a sustainable development strategy holds the potential to enhance productivity, profitability, and overall efficiency by leveraging by-products from other industries. In plaster manufacturing the substitution of natural gypsum with synthetic gypsum is worth exploring. Phosphogypsum (PG) represents a significant fraction of synthetic gypsum production, arising as a by-product of phosphoric acid manufacturing. However, the presence of impurities in PG, particularly phosphorus, poses challenges to its use as a plaster material. To identify the phases present in PG, quantify their occurrences and understand their effects on dehydration and hydration processes, our study aimed to examine simplified models. These models are specifically designed to provide insights into the underlying mechanisms governing the hydration reactivity of hemihydrate. Pure gypsum and brushite were synthesized, and mechanical mixing was carried out to explore how brushite affects the characteristics of gypsum. Additionally, a solid solution of $Ca(SO_4)_{1-x}(HPO_4)_x{\cdot}2H_2O$, where $0 < x < 1$, was prepared to characterize and quantify the syncrystallized HPO_4^{2-} as well as the effects of this impurity on typical gypsum use cases. The synthesized materials underwent physical and chemical characterization using SEM, XRD, IR spectroscopy, DSC, pH and conductivity measurements, and ion chromatography. The results demonstrated that the HPO_4^{2-} ions can substitute for sulfate ions in gypsum to form solid solutions. The maximum quantity of HPO_4^{2-} ions in the gypsum lattice is approximately 10%, leading to the crystallization of gypsum into sand rose shape rather than needle crystals. As the concentration of HPO_4^{2-} ions increases, a new phase known as ardealite ($Ca(SO_4)_{1-x}(HPO_4)_x{\cdot}2H_2O$) with $0.42 < x < 0.54$ emerges, followed by brushite ($CaHPO_4{\cdot}2H_2O$). During the calcination of brushite at 160 °C, a mixture of brushite and monetite formed that exhibits different properties compared to its natural counterpart. In the presence of syncrystallized HPO_4^{2-} ions, the transformation from anhydrite III to anhydrite II occurred at higher temperatures than for pure gypsum. The reactivity of calcined samples indicate that HPO_4^{2-} ions from the dehydration products of brushite caused a delay in hydration, with the maximum delay observed at a calcination temperature of 160 °C. At this temperature, monetite begins to crystallize, and it is characterized by its inert nature, exhibiting no reactivity with water. This explains the observed decrease in setting times as the calcination temperature rises. Moreover, syncrystallized HPO_4^{2-} ions induced a significant delay in the hydration process. Our research revealed that adjusting the calcination temperature can mitigate the retarding effect associated with this impurity, suggesting an industrial tendency to use the lowest possible temperature during the calcination process of PG containing syncrystallized phosphate impurity. In addition, we have observed that adjusting the pH of the mixing water to lower values can significantly accelerate setting times.

* Corresponding author.
E-mail address: nils.haneklaus@donau-uni.ac.at (N. Haneklaus).

https://doi.org/10.1016/j.jclepro.2024.142013
Received 16 November 2023; Received in revised form 7 March 2024; Accepted 27 March 2024
Available online 29 March 2024

1. Introduction

During the production of phosphoric acid with the wet manufacturing process considerable amounts of phosphogypsum (PG) are generated as a residual byproduct (Becker el al., 1989). This procedure entails the reaction of sulfuric acid with rock phosphate as indicated in (1):

$$Ca_{10}(PO_4)_6F_2 + 10\ H_2SO_4 + 20\ H_2O \rightarrow 10\ CaSO_4{\cdot}2H_2O + 6\ H_3PO_4 + 2HF \quad (1)$$

(Bilal et al., 2023)

Approximately 4.5–5.5 metric tons (t) of PG are produced per ton of wet-process phosphoric acid (Jin et al., 2023). The worldwide production of PG is estimated to be within the range of 100–300 million t per year (Oumnih et al., 2019; Rosales et al., 2020). Globally, a substantial proportion, roughly 85%, of PG produced is stored in expansive piles near fertilizer factories (Qi et al., 2023). Without proper treatment storing of PG can lead to soil contamination, polluting of both underground and surface waters after rainfall (Akfas et al., 2024; Tayibi et al., 2009). Furthermore, the accumulation of PG in stockpiles often results in dust issues that require attention to improve environmental conditions (Płachciak, 2020). Additionally, releasing moisture and fine particles from PG into the atmosphere poses risks, as it can carry hazardous pollutants such as radioactive materials, cadmium, mercury, and phosphorus (Akfas et al., 2024a; Rutherford et al., 1996). At present only 15% of the produced PG is recycled through various methods such as the use as a cement retarder (Costa et al., 2022; Potgieter et al., 2003), as a backfill material (Gu et al., 2020) or as a soil conditioner (Bian et al., 2022; Degirmenci et al., 2007). These applications typically involve adding a limited amount of PG, ranging from 5% to 30%, to the primary raw materials.

As the global shift towards renewable energy gains momentum, there is a foreseeable reduction in the demand for coal-fired power plants, leading to a consequent decrease in the production of Flue Gas Desulfurization (FGD) gypsum, as outlined by Haneklaus et al. (2022). PG, characterized by its high-grade gypsum composition as reported by Geraldo et al. (2020), Jin et al. (2020) and Qin et al. (2023a), contains over 95% of calcium sulfate dihydrate ($CaSO_4{\cdot}2H_2O$). It can undergo calcination to produce hemihydrate phosphogypsum (HPG) ($CaSO_4{\cdot}½H_2O$), presenting itself as a promising alternative to natural gypsum and FGD gypsum, carrying substantial practical significance. Furthermore, PG exists in the form of powdered particles, conveniently stacked, making it more accessible than natural gypsum that first needs to be mined (Saadaoui et al., 2017). The utilization of already powdered particles eliminates the need for energy-intensive crushing and grinding processes, resulting in reduced energy consumption compared to the use of natural gypsum ore.

Beyond its application as a gypsum resource, PG is recognized as a potentially valuable source of rare earth elements (REEs) (Bilal et al., 2023; Cánovas et al., 2019; Grabas et al., 2019; Hakkar et al., 2021; Rychkov et al., 2018). Scholars revealed that, during the wet phosphoric acid processing of phosphate rocks with varying REE grades, a significant portion (60–90%) of the initial REE content of the rock phosphate transfers to the PG (Walawalkar et al., 2016). This adds to the appeal of PG as a strategic resource in the presently evolving energy landscape. Consequently, exploring efficient methods for using PG in large quantities in countries where resources are either scarce or non-existent, either as a source of gypsum or as a source of REEs, has recently attracted interest.

The composition of phosphate rock significantly impacts the characteristics and quality of PG that results from its processing. PG primarily consists of $CaSO_4{\cdot}2H_2O$ and minor amounts of silica, typically in form of quartz, alongside various impurities including heavy metals like arsenic (As), cadmium (Cd), chromium (Cr), mercury (Hg), and radioactive materials such as radium (Ra) and uranium (U) (Bilal et al., 2023; Burnett et al., 1996; Kuzmanović et al., 2021; Qin et al., 2023b; Rashad, 2017; Rutherford et al., 1996; Tayibi et al., 2009a). Additionally, PG contains between 0.1% and 1.5% of fluorine (F) and from 0.1% to 1.8% of phosphorus (P_2O_5). The P impurities in PG exist in three forms: soluble, syncrystallized and insoluble P (Ennaciri and Bettach, 2023; Jia et al., 2021; Singh et al., 1993, 1996). Soluble P can be found in various forms, including phosphoric acid (H_3PO_4), monocalcium phosphate monohydrate ($Ca(H_2PO_4)_2{\cdot}H_2O$), and others. Syncrystallized P occurs when brushite ($CaHPO_4{\cdot}2H_2O$) integrates into the lattice of gypsum ($CaSO_4{\cdot}2H_2O$), forming a solid solution due to similarities in size, molar mass, and charge. This substitution allows HPO_4^{2-} ions to replace for SO_4^{2-} ions within the gypsum structure, leading to the formation of ardealite ($Ca_2(HPO_4)(SO_4){\cdot}4H_2O$) (Ennaciri and Bettach, 2018). The substitution process is influenced by factors such as sulfuric acid concentration, reaction time, and mixing temperature during phosphoric acid production. Additionally, insoluble phosphate compounds, such as tricalcium phosphate ($Ca_3(PO_4)_2$), are generated in the process.

Recycling PG to replace natural gypsum and FGD gypsum in the construction industry could be a promising way to advancing sustainable practices while decreasing resources dependencies. Nevertheless, it has been found that impurities in the PG, particularly P impurities, hinder its direct use as a building material. P adversely affects the hydration and solidification processes of HPG, resulting in lower gypsum dihydrate precipitation rates, longer setting times and reduced strength if compared to data from natural gypsum (Abdelhadi et al., 2014; Altun and Sert, 2004; Bagade and Satone, 2012; Huang and Lin, 2011; Ölmez and Erdem, 1989; Taher, 2007; Zhou et al., 2020). Previous research, such as that carried out by Singh (2003), has investigated the impact of P impurities on the properties of gypsum. Singh identified a sequence of influences, considering factors like setting time and compressive strength, as follows: $H_3PO_4 > Ca(H_2PO_4)_2{\cdot}H_2O > CaHPO_4{\cdot}2H_2O > Ca_3(PO_4)_2$. In addition, these impurities were observed to modify the morphology of the crystal grains in plaster hydration products. Needle-shaped crystals, in contrast to prismatic crystals of short length and irregular boundaries, contribute to greater compressive strength (Singh, 2005). In a recent study by Jia et al. (2021), it was further found that a higher concentration of H_3PO_4 on the PG surface could expedite the setting time while reducing the 2-h strength of HPG plaster.

Several researchers are investigating pre-treatment techniques to counteract the negative effects of P impurities and improve the recyclability of PG. Soluble P impurities have been effectively removed from PG by washing processes, while insoluble P impurities have been effectively sieved out. In the case of syncrystallized P impurities, a unique strategy involving high-temperature calcination technology was deployed, enabling them to be transformed into insoluble pyrophosphate compounds (Liu et al., 2018; Ma et al., 2020; Peng et al., 2021). Treatment with citric acid, used by Singh (2002) also removed impurities and yielded favorable results. However, the role of P as a retardant has an impact on the setting time (Möschner et al., 2009). A modification technique was developed to eliminate P impurities from PG through the utilization of lime (Chen et al., 2019; Liu et al., 2020). The lime neutralization method effectively addressed the problem of soluble P impurities delaying cement setting times. It was, however, inefficient at eliminating insoluble and syncrystallized P impurities. Cai et al. (2021) found that PG could be purified using 1% $H_2C_2O_4$. Nevertheless, this purification method has certain drawbacks, significantly limiting its industrial application. The acidity of PG can lead to corrosion of construction equipment and facilitate mold growth. Moreover, HPG is prone to moisture and mildew, as observed by Chen et al. (2019). Ennaciri et al. (2020) presented a method for purifying PG using sulfuric acid to dissolve insoluble impurities. Their findings indicate that a 20% sulfuric acid treatment is sufficient to render PG suitable for the gypsum industry. However, for applications in the cement industry, a higher concentration of up to 50% sulfuric acid, is required to effectively treat PG and remove impurities, as noted by Moalla et al. (2018). It is important to note that an excessively high concentration of sulfuric acid can lead to the dehydration of gypsum into anhydrous gypsum (AH). AH

Table 1
The reagents employed in the synthesis of gypsum and brushite.

Products	K_2SO_4	K_2HPO_4	$CaCl_2{\cdot}2H_2O$
Origin	Alfa Aesar	Prolabo	Prolabo
Concentration (g/100 ml)	6	5	50
pH	6.6	9.2	6.4

poses challenges as a cement retarder due to its slow hydration rate, which can result in the secondary formation of ettringite. This secondary ettringite formation can cause expansion and even result in the rupture of the cement-hardened structure (Allevi et al., 2016; García-Maté et al., 2015; Winnefeld and Lothenbach, 2010).

In practical terms, the aforementioned treatments prove effective in eliminating a portion of impurities. The removal of soluble impurities is relatively straightforward, but addressing syncrystallized impurities poses a more significant challenge. Implementing the aforementioned methods can also lead to increased investment and production costs (Chen et al., 2019). To tackle this, adjustments to existing phosphoric acid production facilities would often be necessary. This approach has been implemented in Japan, a country lacking natural gypsum, where phosphoric acid production processes had to be modified to produce PG suitable for plasterboard manufacturing. The complete sequence of PG treatment operations significantly impacts the cost of the final product.

Additionally, it should be noted that a method developed for a specific PG deposit might be entirely ineffective for another one since the impurities can significantly vary depending largely on the phosphate rock used as raw material in the production process. As a result, the limited utilization rate of PG makes complete utilization in the short term nearly impossible, posing a significant global challenge due to the storage of PG and its possible contribution to the pollution in water, land, and atmosphere (Chernysh et al., 2021).

To meet the standards necessary for utilization of PG in plaster manufacturing, PG must have an appropriate morphology and contain minimum levels of P, while ensuring that it remains as free as possible from radionuclides and fluorine. Given the difficulty in removing syncrystallized P and the mechanisms through which these impurities affect PG properties remain ambiguous. The research presented here is designed to characterize the syncrystallized P and to identify the phases in which P occurs in gypsum, quantify the occurrences and further study their influences on the hydration reactivity of hemihydrate. To achieve these objectives, it was necessary to use simplified models to better understand the influence of the impurities on the more complex PG. For this purpose, we synthesized gypsum and brushite and carried out mechanical mixing experiments to explore the influence of brushite on gypsum characteristics and PG properties. In addition, we synthesized a solid solution of $Ca(SO_4)_{1-x}(HPO_4)_x{\cdot}2H_2O$, where $0 < x < 1$, to understand how to characterize and quantify these impurities and study their effect on gypsum.

2. Materials and methods

2.1. Preparation of reference products

Gypsum and brushite were synthesized, along with a solid solution of $Ca(SO_4)_{1-x}(HPO_4)_x{\cdot}2H_2O$ with $0 < x < 1$, via a precipitation method. The reagents used in our experiments were obtained from Alfa AESAR and PROLABO and their characteristics are summarized in Table 1.

The reference products were synthesized according to the procedure described by Guilhot et al. (1974). Gypsum was synthesized through the precipitation of potassium sulfate using an excess of calcium chloride dihydrate, following reaction (2):

$$\begin{gathered} K_2SO_4 + CaCl_2{\cdot}2H_2O \rightarrow CaSO_4{\cdot}2H_2O + 2KCl \\ (1-X)\,2\left[K^+ + SO_4^{2-}\right] + \left[Ca^+ + 2CI^- + 2H_2O\right] \rightarrow 2K^+ + 2CI^- + \left[Ca^{2+} + SO_4^{2-} + 2H_2O\right]_{gypsum} \end{gathered} \quad (2)$$

Calcium monohydrogen phosphate dihydrate, also known as brushite ($CaHPO_4{\cdot}2H_2O$), is produced through a precipitation process involving the combination of potassium phosphate and calcium chloride dihydrate, according to the reaction:

$$\begin{gathered} K_2HPO_4 + CaCl_2{\cdot}2H_2O \rightarrow CaHPO_4{\cdot}2H_2O + 2KCl \\ X\left[2K^+ + HPO_4^{2-}\right] + \left[Ca^{2+} + 2CI^- + 2H_2O\right] \rightarrow 2K^+ + 2CI^- + \left[Ca^{2+} + HPO_4^{2-} + 2H_2O\right]_{brushite} \end{gathered} \quad (3)$$

The precipitates were filtered using a fritted glass and then rinsed with distilled water to eliminate traces of KCl and NaCl. After that, they were dried with ethanol and stored in the oven at 40 °C.

2.2. Synthesis of the solid solution

The solid solution gypsum–brushite was also synthesized using the method outlined by Guilhot et al. (1974). The reagents used and the concentration of the solutions are the same as in the preparation of the pure reference products. Calcium chloride was added to the previously stirred mixtures. The precipitates obtained were filtered on sintered glass, then washed with distilled water, dried in air, and kept in an oven at 40 °C for at least 24 h.

The solid solution between $CaSO_4{\cdot}2H_2O$ and $CaHPO_4{\cdot}2H_2O$ was obtained by adding potassium sulfate and potassium phosphate with calcium chloride dihydrate in excess following the two simultaneous reactions by varying the molar contents of HPO_4^{2-}:

$$\begin{aligned} (1-X)\left[2K^+ + SO_4^{2-}\right] + \left[Ca^{2+} + 2CI^- + 2H_2O\right] &= (1-X)2K^+ + 2CI^- + \left[Ca^{2+} + XHPO_4^{2-} + 2H_2O\right] \\ X\left[2K^+ + HPO_4^{2-}\right] + \left[Ca^{2+} + 2CI^- + 2H_2O\right] &= 2XK^+ + 2CI^- + \left[Ca^{2+} + XHPO_4^{2-} + 2H_2O\right] \end{aligned} \quad (4)$$

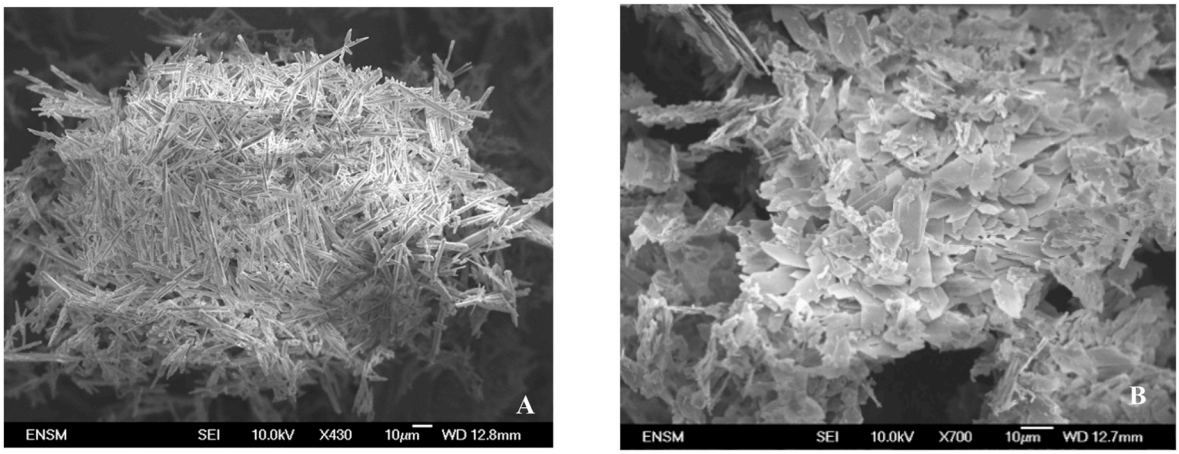

Fig. 1. SEM images of reference products (A) gypsum and (B) brushite.

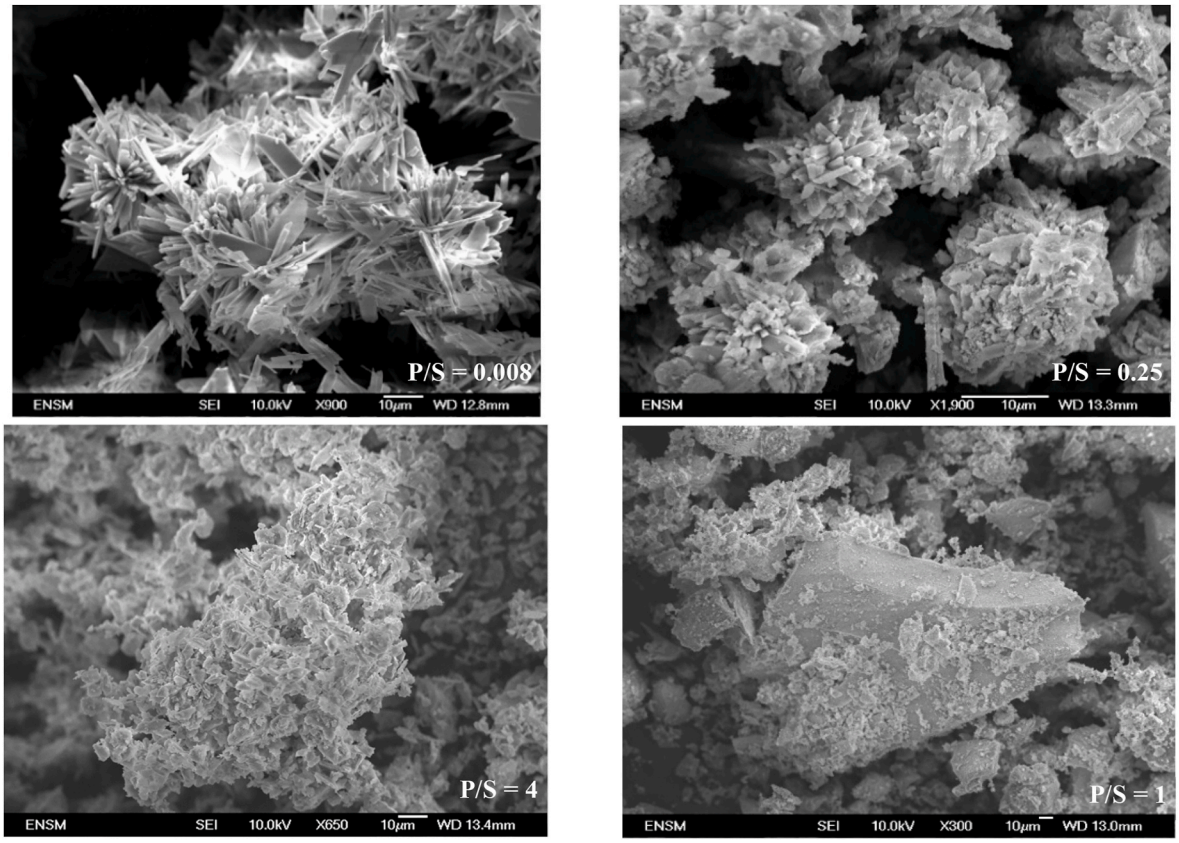

Fig. 2. SEM images of the solid solution obtained by precipitation at different P ion concentrations: P/S = 0.008 (top left), P/S = 0.25 (top right), P/S = 4 (bottom left), and P/S = 1 (bottom right).

The solid solution obtained corresponds to the chemical formula $Ca(SO_4)_{1-x}(HPO_4)_x{\cdot}2H_2O$, where "x" is the molar proportion of HPO_4^{2-} in the solid solution.

2.3. Methods

The samples were analyzed using a scanning electron microscope (SEM) (JEOL JSM-840) equipped with an energy dispersive X-ray spectrometer (Tracor Northern TN-2000). Prior to analysis, the surface of the samples was coated with a double layer of gold.

X-ray powder diffraction analyses were conducted using a Siemens D-5000 Kristallofex diffractometer equipped with a copper anticathode. The radiation ($Cu_{K\alpha}$, $\lambda = 1.54056$ Å) was filtered with Ni. The accelerating voltage was set to 40 KV, for a current of 30 mA. The slit system was set at 1-0, 1-1 mm for a receiving slit of 0.6 mm. The data were collected in the 5–90° (2θ) range with a step width of 0.02° (2θ) and a step time of 2s. Consistent operating conditions were upheld for the High-temperature XRD Brucker (AXS) D8 Advance automatic diffractometer, under a helium flow rate of 20 ml/min. The heating rate was set at 10 °C/min.

Infrared absorption spectroscopy measurements were performed using two different instruments: a SPECORD M-80 non-Fourier transform spectrometer, which operated in the frequency range of 250–4000 cm^{-1}, and a THERMO NICOLET NEXUS Fourier transform spectrometer,

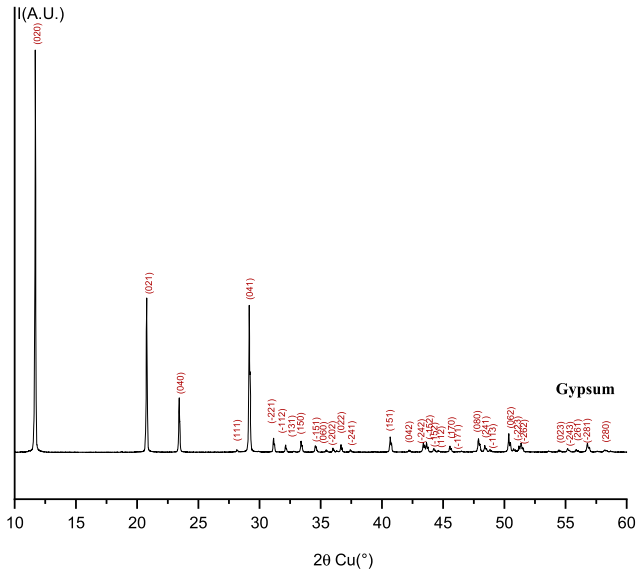

Fig. 3. X-ray diffraction pattern of gypsum, with diffraction reflections indexed based on ICDD card no. 00-033-0311.

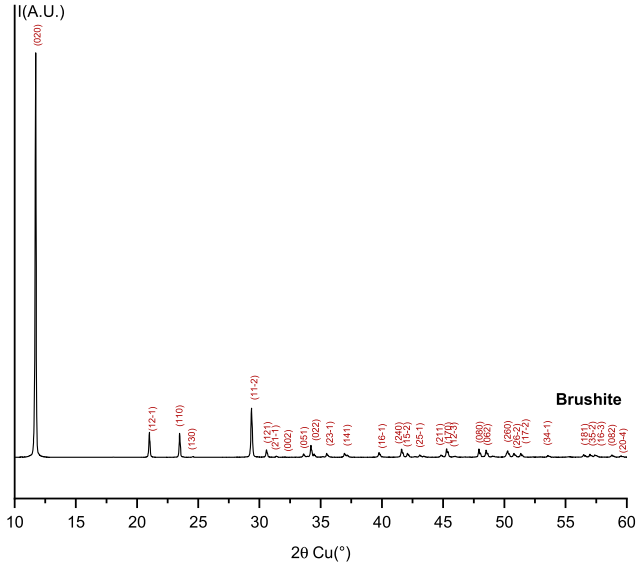

Fig. 4. X-ray diffraction pattern of brushite, with diffraction reflections indexed based on ICDD card no. 04-013-3344.

which functioned in the frequency range of 400–4000 cm^{-1}.

The dehydration of samples was conducted using a SETRAM TAG 24 dual-furnace thermobalance coupled with a DSC 111 thermal analyzer, allowing for simultaneous recording of TGA and DSC thermogravimetric curves. The heating rate was set at 10 °C/min in a continuous flow of argon at a rate of 30 ml/min. The evolved gases were collected and analyzed by infrared adsorption spectroscopy using a BIORAD FTS 40 spectrometer.

3. Results and discussion

3.1. Morphology analysis

The gypsum synthesized via precipitation presents a needle-like structure, as depicted in Fig. 1A. The crystals are uniformly distributed both in terms of their size and shape. These observations align with the results reported in the investigations conducted by Klepetsanis and Koutsoukos (1998), Mahmoud et al. (2004) and Shih et al. (2005). Pure brushite displays a pseudo parallelepiped-shaped plate morphology, as seen in Fig. 1B. The crystals have a tabular form along the (010) axis and appear elongated along either the (101] or (102] axes. The brushite crystals obtained in this study are comparable to those synthesized at pH values of 4.8–5.0, pH = 7, and pH between 5.5 and 7, as reported in the studies of Abbona Christensson et al. (1993), Arifuzzaman and Rohani (2004) and Toshima et al. (2014).

The solid solution exhibits a distinctive sand rose-like morphology (Fig. 2), whereby the crystals clustered into polycrystalline aggregates. When the concentration of HPO_4^{2-} ions increased, the crystals thickened forming more compact aggregates. At a P/S ratio of 4, the crystal morphology of the solid solution is similar to that of brushite. However, the platelets are slightly thicker and less well-shaped. In the case of a P/S ratio of 1, the solid solution is a powder, poorly crystallized and presented in the form of large, deformed, and compact grains. This compound is also found as a natural mineral species and is known as ardealite (Dumitraş, 2017; Onac et al., 2005).

3.2. XRD analysis

The similarity between gypsum, matching with the ICDD card no.00-033-0311, and brushite, aligning with the ICDD file no. 04-013-3344, is evident in Figs. 3 and 4, where their diffraction patterns show nearly identical unit cells. This resemblance poses a significant challenge in X-ray diffraction studies of the gypsum-brushite system, as the crystallographic similarities between these two minerals can make it difficult to distinguish them accurately. Particularly, the highest peaks of brushite and gypsum overlap for $d(020)$, corresponding to $2\theta = 11.7°$. Hence, to discriminate between these two phases, it is necessary to examine the diffraction peaks relating to $d(021)$, corresponding to $2\theta = 20.7°$ for gypsum, and $d(12\text{-}1)$, corresponding to $2\theta = 21.0°$ for brushite. Notably, the two peaks can only be differentiated when the content of brushite exceeds 1% in the gypsum-brushite mixture. Many scholars considered the characterization of powder mixtures composed of gypsum and brushite (ranging from 0% to 1%) by X-ray diffraction to be extremely difficult. Roode-Gutzmer and Strydom (1999) for instance assert that the heights and areas of bands corresponding to the (022) reflection at $2\theta = 34.2°$ (although a common peak with a peak of gypsum) are proportional to the percentage of brushite present.

The XRD technique is essentially unable to detect the presence of brushite or any other phosphate phase in products containing less than 5% of monohydrogen phosphate HPO_4^{2-} ions. In such cases, only the gypsum phase is present, as shown in Fig. 5. However, when the concentration of phosphate ions in the solid solution exceeds 7%, demixing occurs. This results in the emergence of a new phase, $Ca_2(SO_4)(HPO_4)\cdot 4H_2O$, identified as the ardealite phase, alongside gypsum. Subsequently, between phosphate ion contents of 40% and 55%, gypsum disappears and only the ardealite phase remains. These findings are also consistent with the research conducted by Pinto et al. (2011). In the range of 55%–95% HPO_4^{2-} content, ardealite coexists with brushite. However, beyond this range, only brushite is observed. Rinaudo et al. (1996) also explored a portion of this phase diagram (for $50\% < HPO_4^{2-} < 100\%$) through analysis of their samples using XRD and EDS. Their findings closely resemble the results obtained during this study (at the same pH), except for the range $65\% < HPO_4^{2-} < 100\%$. According to their research, only the brushite phase is present within this range. However, in our study, both brushite and ardealite phases were present. It is noteworthy that it is only when the HPO_4^{2-} concentration surpasses 97% that ardealite disappears in our case.

It has been observed that the presence of syncrystallized HPO_4^{2-}-bearing phases cannot be demonstrated by the XRD technique at concentrations below 10%. Similarly, the existence of brushite at concentrations below 1% in a mixture with gypsum cannot be proven through this characterization method. Therefore, the products were characterized using IR spectroscopy, providing an alternative approach to

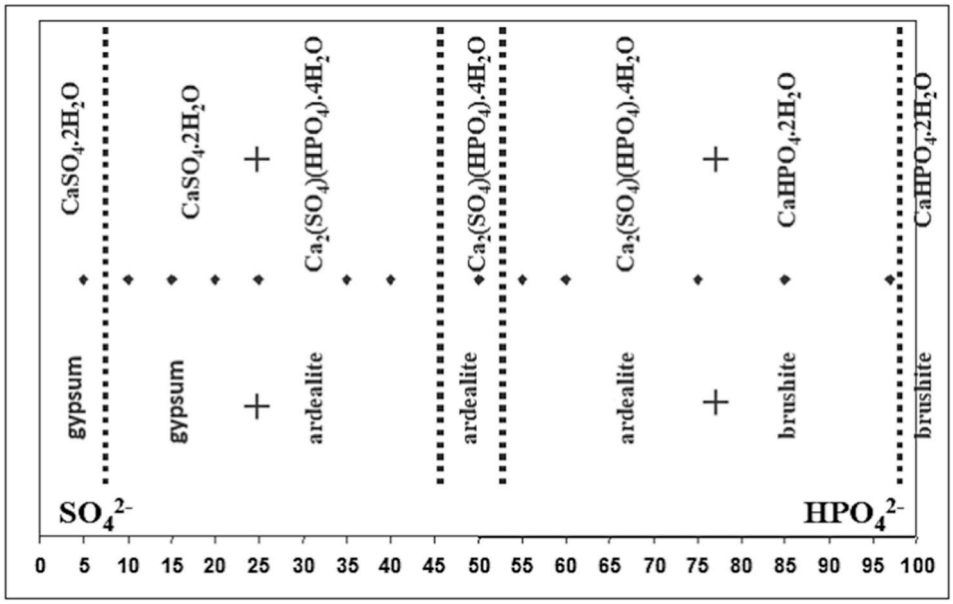

Fig. 5. Order of appearance of the phases according to the variation of the HPO_4^{2-} contents, inferred by XRD analysis.

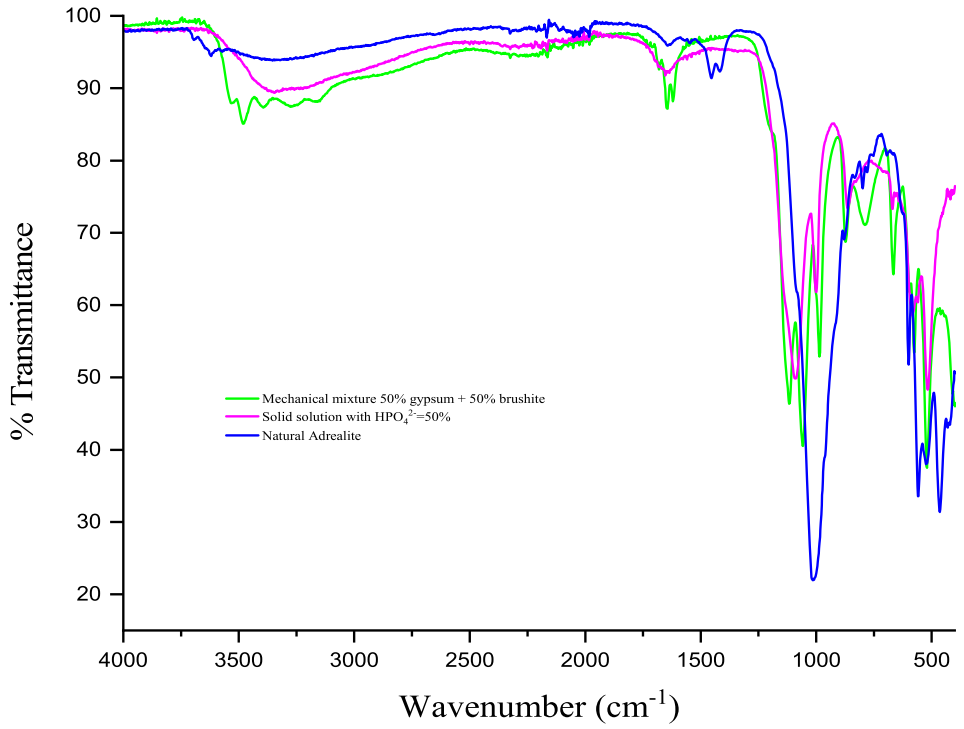

Fig. 6. Infrared spectra of mechanical mixture of 50% gypsum and 50% brushite, and solid solution with HPO_4^{2-} = 50% and natural ardealite (Cioclovina Uscata cave).

investigating their structure. Moreover, IR spectroscopy facilitates quantitative analysis of syncrystallized ions, providing valuable insights into the composition of the samples.

3.3. IR spectroscopy

The IR spectrum of a solid provides information on its structure (geometry, interatomic forces, inter- and intramolecular forces, etc.). In the solid phase, the substitution of certain ions from a pure solid by ions of similar structure leads to the formation of a solid solution. The presence of these ions disturbs existing bonds and generally forms new ones, which leads to the appearance of absorption bands in addition to those of the pure solid. Therefore, qualitative analyses can be carried out using IR spectroscopy. Moreover, since the intensity of the absorption bands of a molecular species is proportional to the concentration of that substance in the sample, IR spectroscopy enables quantitative analysis of syncrystallized ions.

The IR spectra of the mechanical mixture composed of 50% gypsum and 50% brushite, the solid solution with HPO_4^{2-} = 50%, as well as the natural ardealite, are depicted in Fig. 6. The IR spectrum of the mechanical mixture reveals distinct bands corresponding to the characteristics of gypsum and brushite (Table 2). While the spectra of natural

Table 2
Positions and assignments of IR absorption bands for gypsum, brushite and ardealite.

(cm^{-1}) Type of vibration	Wavelength		
	Gypsum	Brushite	Ardealite
Stretching vibrations υO-H of water	3540–3251	3542–3166	Poorly resolved
Stretching vibrations υ(P)O–H of HPO_4^{2-}	–	2930–2347	2972–2322
Stretching vibrations υO-S-O of SO_4^{2-}	2217–2118	–	–
Bending vibrations δO-H of water	1682–1620	1742–1650	1708–1645
Bending vibrations υP-O-H	–	1212	1194
Stretching vibrations υP-O of PO_4^{3-} (υ_3 and υ_1)	–	1135–986	–
Stretching vibrations υO-S-O of SO_4^{2-} (υ_3 and υ_1)	1099–1004	–	–
Stretching vibrations υO-S (P)–O of SO_4^{2-} and HPO_4^{2-} (υ3 and υ1)	–	–	1134–961
Stretching vibrations υ(P)O–H	–	872	864
Bending vibrations P–O(H) of HPO_4^{2-}	–	795	824
υ_2 H–O–H	–	670–662	–
υ_2 H–O–H + υ_4 O–S–O	–	–	672–637
Bending vibrations O–S–O of SO_4^{2-} (ν_4)	666–594		–
υ_4 O–P–O + υ_4 O–S–O	–	–	596
Bending vibrations PO_4^{3-} (υ_4 and υ_2)	–	577–403	–
Bending vibrations υ_4 O–P–O of HPO_4^{2-}	–	–	560–525
Bending vibrations υ_2 O–P(S)–O	–	–	424

Table 3
Summary of the wavelengths corresponding to the absorption bands of HPO_4^{2-} observed on the IR spectra of gypsum solid solution and gypsum-brushite mixture.

Form of HPO_4^{2-}	Characteristic bands of HPO_4^{2-} in wavelengths (cm^{-1})			
HPO_4^{2-} (brushite)	1650	986	872	524
HPO_4^{2-} syncristallized	**1017**		**836**	

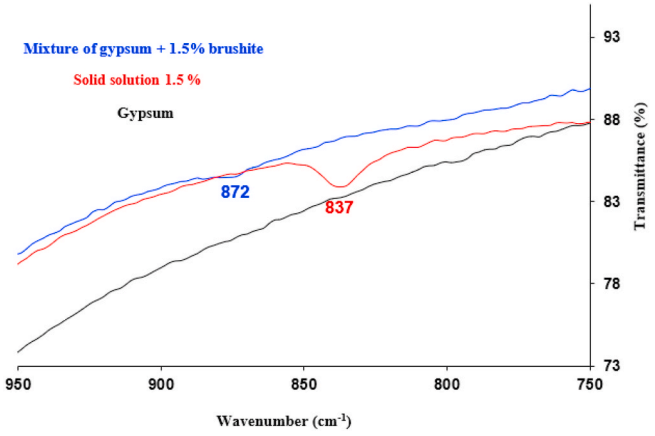

Fig. 7. Infrared absorption spectra of gypsum and 1.5% brushite mixture (blue), solid solution containing 1.5% of HPO_4^{2-}(red), and the reference curve of pure gypsum (black). (For interpretation of the references to colour in this figure legend, the reader is referred to the Web version of this article.)

and synthetic ardealite are very similar, they differ from the spectrum of the 50% gypsum and 50% brushite mixture. It should be noted that the absorption band attributed to symmetrical stretching of P–O(H) in the 800-900 cm^{-1} range is located at 872 cm^{-1} for brushite and 864 cm^{-1} for ardealite. Therefore, IR spectroscopy allows distinguishing mechanical mixtures of gypsum and brushite from an ardealite-type phase that contains equal proportions of HPO_4^{2-} and SO_4^{2-} ions. The band assignments of gypsum, brushite and ardealite, as presented in Table 2, are attributed to the investigations carried out by Dumitras et al. (2004), Anbalagan et al. (2009), and Dumitraş (2017).

Even at a low concentration of only 1.5% within gypsum, brushite can be detected by IR spectroscopy because of its distinctive absorption band at 872 cm^{-1} (Table 3 and Fig. 7). This specific band corresponds to the symmetric non-degenerate PO stretching mode present in the HPO_4^{2-} structural group. If the gypsum-brushite mixture is homogeneous, the height of this absorption band can be correlated with the quantity of brushite introduced (Fig. 8), which is consistent with the study of Aslanian et al. (1980). In contrast to the mechanical mixture of gypsum and brushite, the solid solution containing syncrystallized HPO_4^{2-} ions is distinguished by the existence of two absorption bands: 1017 cm^{-1}, corresponding to the ν_3 vibration [asymmetric stretching P–O(H)] within the $(PO_4)^{3-}$ structural group, and 836 cm^{-1}, corresponding to the ν_1 vibration associated with the HPO_4^{2-} structural group (Table 3). These specific bands can be used to establish a calibration curve. A notable correlation is observed between the quantity of introduced syncrystallized HPO_4^{2-} ions within the gypsum solid solution and the peak height of the absorption band, as illustrated in Fig. 8.

Fig. 9 highlights the pattern of the main absorption band associated with syncrystallized HPO_4^{2-} ions, positioned at 836 cm^{-1}. It demonstrates an increase in intensity up to a concentration of 10% HPO_4^{2-}. Subsequently, as the concentration of incorporated phosphate ions rises, the intensity diminishes and disappears entirely at 30%. Moreover, a band emerges at 864 cm^{-1} when the HPO_4^{2-} concentration exceeds 10%, marking the phase separation of the solid solution containing SO_4^{2-} and HPO_4^{2-} in gypsum into two distinct phases: one comprising HPO_4^{2-}-bearing gypsum and the other containing ardealite. Between 40% and 50% HPO_4^{2-}, only the band at 864 cm^{-1} persists, indicating the presence of the HPO_4^{2-} ion in the ardealite phase. The intensity of this band increases with the rise in percent HPO_4^{2-} and gradually shifts towards higher wavelengths. Specifically, at 80% HPO_4^{2-}, the band is located at 870 cm^{-1} and reaches 872 cm^{-1} for pure brushite.

4. Dehydration of the products

4.1. Dehydration of pure phases

The gypsum dehydration process is an essential step for plaster production. This section of the paper examines the thermal properties of HPO_4^{2-} ions within the $CaO–SO_3–H_2O$ system, focusing on understanding their behavior during the transition from PG to HPG. Through using of DSC, XRD, and IR spectroscopy techniques, the dehydration process of gypsum in the presence of HPO_4^{2-} ions was thoroughly investigated. Fig. 10 depicts the DSC curves of gypsum, brushite, and ardealite.

Gypsum dehydration is characterized by two endothermic peaks, recorded at 144 °C and 167 °C. The first endothermic peak is attributed to the formation of bassanite (hemihydrate):

$$CaSO_4{\cdot}2H_2O \rightarrow CaSO_4{\cdot}\ ½\ H_2O + 3/2\ H_2O\ (144\ °C) \quad (5)$$

The subsequent endothermic peak corresponds to the transformation of the hemihydrate into anhydrite III, indicating a transformation of the crystalline structure (from monoclinic, as in the hemihydrate, to hexagonal, as in anhydrite III):

$$CaSO_4{\cdot}\ ½\ H_2O \rightarrow CaSO_4\ III + ½\ H_2O\ (167\ °C) \quad (6)$$

In addition, an exothermic peak is observed at 356 °C, showing a transformation of the hexagonal structure of anhydrite (III) into an orthorhombic structure known as anhydrite (II):

$$CaSO_4\ III \rightarrow CaSO_4\ II\ (356\ °C) \quad (7)$$

The findings obtained from this study are in good agreement with the research conducted by Engbrecht and Hirschfeld (2016) and Mirwald (2008).

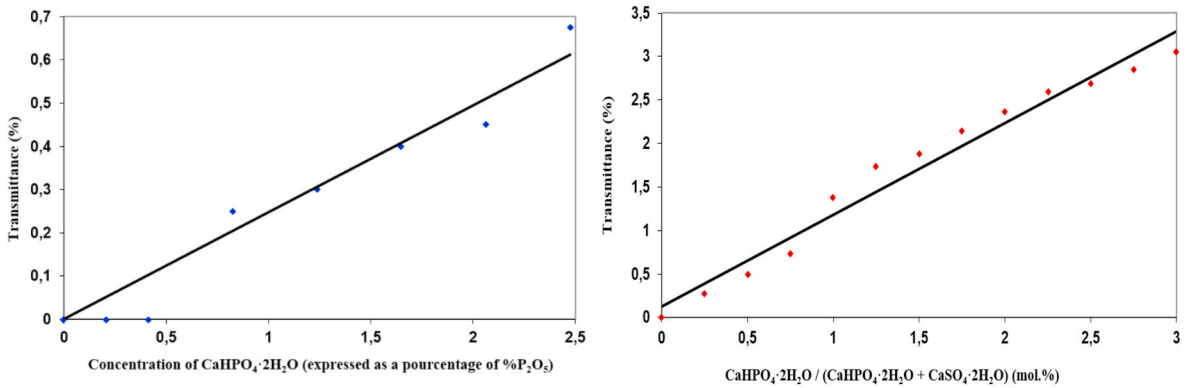

Fig. 8. Correlation between the intensity of the absorption band at 872 cm^{-1} (left) within the gypsum-brushite system, and at 837 cm^{-1} (right) within the solid solution, to the P/S ratio.

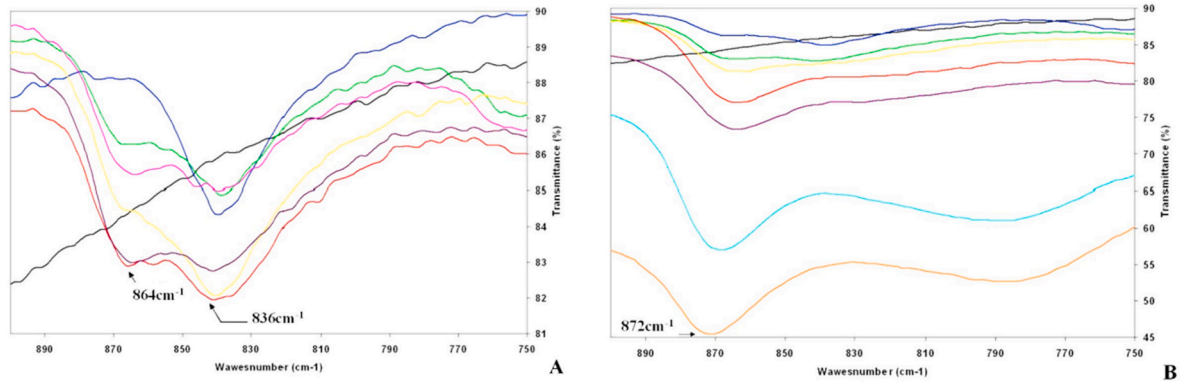

Fig. 9. Infrared spectra of the 900-750 cm^{-1} region of gypsum samples containing 0% < HPO_4^{2-}< 100% $CaSO_4.2H_2O$, % HPO_4^{2-} = 5%, 10%, 12%, 13%, 14%, 20% (Fig A)
$CaSO_4.2H_2O$, % HPO_4^{2-} = 10%, 20%, 30%, 40%, 50%, 60%, 80%, $CaHPO_4.2H_2O$ (Fig B).

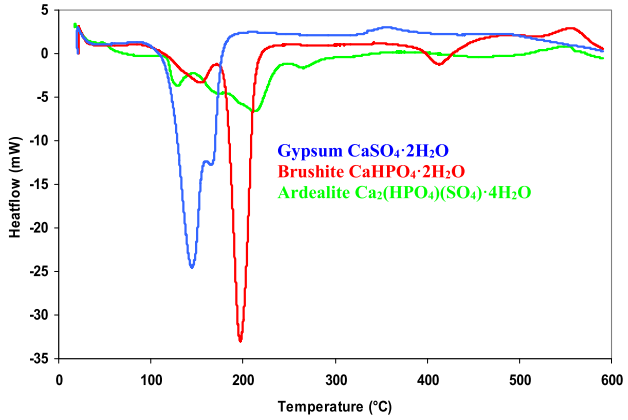

Fig. 10. DSC curves of gypsum, brushite and arderalite

When heated, brushite undergoes a two-step process of losing its molecular water at temperatures of 155 °C and 199 °C. This transformation leads to the conversion of brushite into monetite (Dosen and Giese, 2011):

$$CaHPO_4{\cdot}2H_2O \rightarrow CaHPO_4 + 2H_2O \quad (8)$$

A third endothermic peak is observed around 415 °C. This peak indicates an additional dehydration process attributed to the reaction (Frost and Palmer, 2011):

$$CaHPO_4 \rightarrow Ca_2P_2O_7 + H_2O\ (415\ °C) \quad (9)$$

The exothermic reaction observed in the DSC curve at approximately 555 °C corresponds to the transformation of the amorphous $Ca_2P_2O_7$ product into the crystalline β-$Ca_2P_2O_7$ phase (Dumitras et al., 2004).

Brushite, subjected to varied calcination temperatures, underwent XRD analysis, as depicted in Fig. 11. Within the temperature range of 25–250 °C, only brushite and monetite phases are discerned, while the presence of $Ca_3(PO_4)_2$ and $Ca(H_2PO_4){\cdot}H_2O$ phases remain undetected. Notably, at 260 °C, only monetite is observed. These XRD findings are consistent with the research conducted by Dumitras et al. (2004). According to Lang Dupont, 1985, obtaining pure anhydrous calcium phosphate is impossible. Before dehydration is complete, calcium pyrophosphate begins to form, with an overlap of the two reactions always observed. This hypothesis is confirmed a priori here as indicated in Fig. 11.

During the ardealite dehydration process, several transformations occur. First, ardealite disappears and brushite becomes the dominant compound, accompanied by a minor presence of monetite. The reaction equation for the dehydration process of ardealite can be written as follows:

$$2Ca(HPO_4)(SO_4){\cdot}4H_2O \rightarrow CaHPO_4{\cdot}2H_2O + CaHPO_4 + 2CaSO_4{\cdot}½\ H_2O + 5H_2O\ (130\ °C) \quad (10)$$

At a temperature of 168 °C, hemihydrate transforms $CaSO_4$ III. Upon reaching 215 °C, brushite is entirely replaced by monetite. Within the temperature range of 250–350 °C, both stable anhydrite II and amorphous calcium pyrophosphate are concurrently formed, causing

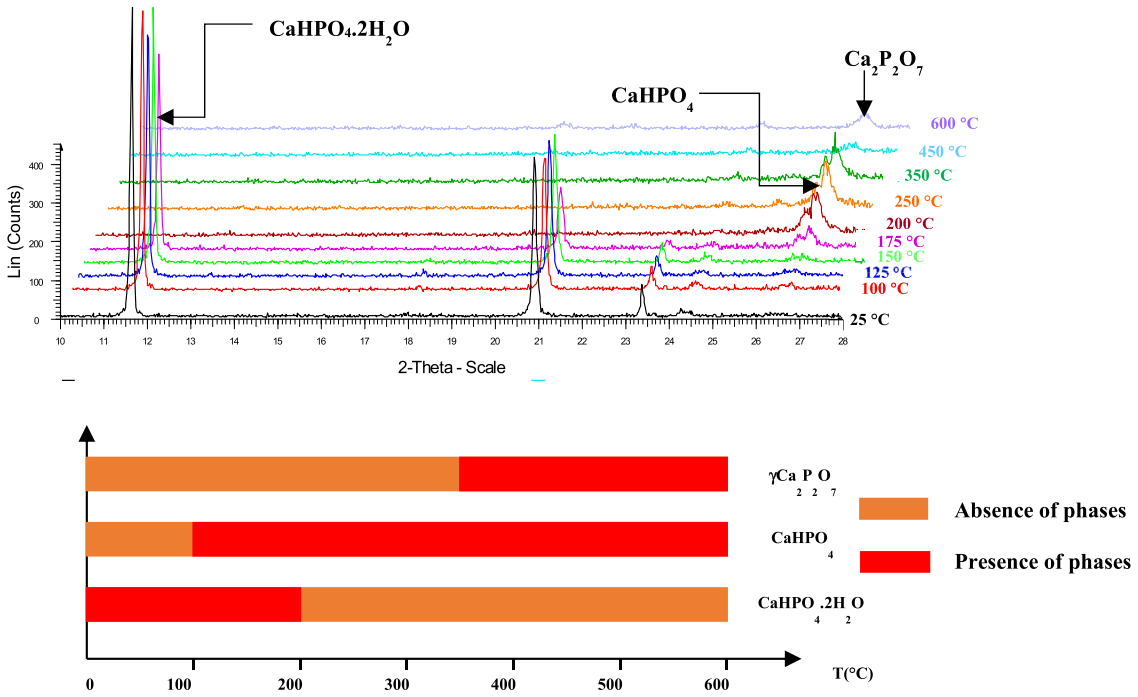

Fig. 11. A series of powder X-ray diffraction patterns taken during the calcination of brushite.

alterations in both $CaSO_4$ and $CaHPO_4$. At 555 °C, the amorphous $Ca_2P_2O_7$ undergoes a transition into the β-$Ca_2P_2O_7$ pyrophosphate phase. This explanation regarding the ardealite (ICDD: 04-011-6882) dehydration process corresponds with the one presented by Dumitraş (2017) and this is confirmed by the results obtained from XRD in situ analyses shown in Fig. 12.

4.2. Dehydration of solid solution

Regarding the dehydration behavior of gypsum with syncrystallized HPO_4^{2-} ions, the solid solution exhibits higher transformation temperatures from anhydrite III to anhydrite II, as shown in Fig. 13. Moreover, the intensity of the exothermic peaks diminishes progressively with an increase in the HPO_4^{2-} concentration within the solid solution. Eventually, at 5% of HPO_4^{2-}, the peaks become barely noticeable, as elucidated in Fig. 14A. In addition, several interesting observations can be noted in Fig. 14. At an HPO_4^{2-} concentration of 10%, the thermogravimetric analysis reveals the emergence of two distinct endothermic peaks at 185 °C and 220 °C. Moreover, when the HPO_4^{2-} content reaches 40%, the thermogravimetric curve suggests a predominance of gypsum in the sample. In contrast, the thermogravimetric curve for an 80% HPO_4^{2-} concentration predominantly indicates the presence of brushite (Fig. 14B).

A phase diagram for the $CaSO_4{\cdot}2H_2O$ - $CaHPO_4{\cdot}2H_2O$ system at 150 °C can be derived from a thorough comprehension of the dehydration processes of gypsum, brushite, ardealite, and their intermediates. This diagram, as depicted in Fig. 15, was derived from XRD analyses conducted on the calcined samples, carried out under a nitrogen flow for 5 h. These analyses were instrumental in establishing the phase diagram for the $CaSO_4{\cdot}2H_2O$ - $CaHPO_4{\cdot}2H_2O$ system at 25 °C that is illustrated in Fig. 4.

To accurately represent the diagram, it was necessary to divide the second part of the diagram, where both bassanite, brushite, and monetite phases are present, into two sections: For compositions with 7% < $CaHPO_4{\cdot}2H_2O$ < 55%, the predominant phase is bassanite hemihydrate, accompanied by the presence of monetite and brushite. For compositions with 55% < $CaHPO_4{\cdot}2H_2O$ < 97%, the prevalent phase is monetite, with the presence of brushite and bassanite. In the cases when 0% < $CaHPO_4{\cdot}2H_2O$ < 7%, only bassanite is detectable via XRD. However, the syncrystallized HPO_4^{2-} ions are still present even after calcination, which was confirmed by IR spectroscopy (Fig. 16). This observation aligns with the findings previously reported by Li and Zhang (2021).

5. Hydration of the products

The main objective of this section of the study is to investigate the hydration reactivity of the obtained products. For this purpose, the materials were subjected to a 5-h calcination in a nitrogen atmosphere at 150 °C, followed by a 24-h reversion period at room temperature. This treatment aimed to produce a hemihydrate with embedded phosphate. Subsequently, we focused on the hydration of these plasters and, to fully understand their reactivity, we used conductivity measurements coupled with pH meter readings. A water-to-phosphoplaster ratio of 20 (W/PP = 20) was maintained throughout all conductometry experiments.

Prior to addressing the hemihydrate and phosphate mixtures, our initial emphasis is on comprehending the hydration processes of hemihydrate, brushite, and monetite. This foundational understanding precedes a more in-depth exploration into the hydration of a more complex system, specifically CaO-SO_4-HPO_4-xH_2O.

Gypsum plaster is produced by calcining calcium sulfate dihydrate and subsequently hydrating the resulting calcium sulfate hemihydrate. During the hydration process of calcium sulfate hemihydrate, the following reaction takes place:

$$CaSO_4{\cdot}½\ H_2O\ (s) + 3/2\ H_2O \rightarrow CaSO_4{\cdot}2H_2O \quad (11)$$

This reaction is only achievable in liquid water, and we adhere to the reaction scheme proposed by Le Chatelier, suggesting that hydration proceeds through two successive reactions that quickly become simultaneous:

Dissolution of the hemihydrate:

$$CaSO_4{\cdot}½\ H_2O_{(s)} \rightarrow Ca^{2+}_{(aq)} + SO^{2-}_{4\ (aq)} + ½\ H_2O_{(aq)} \quad (12)$$

Precipitation of gypsum:

$$Ca^{2+}_{(aq)} + SO_4^{2-}{}_{(aq)} + 2\ H_2O_{(aq)} \rightarrow CaSO_4{\cdot}2H_2O_{\ (s)} \quad (13)$$

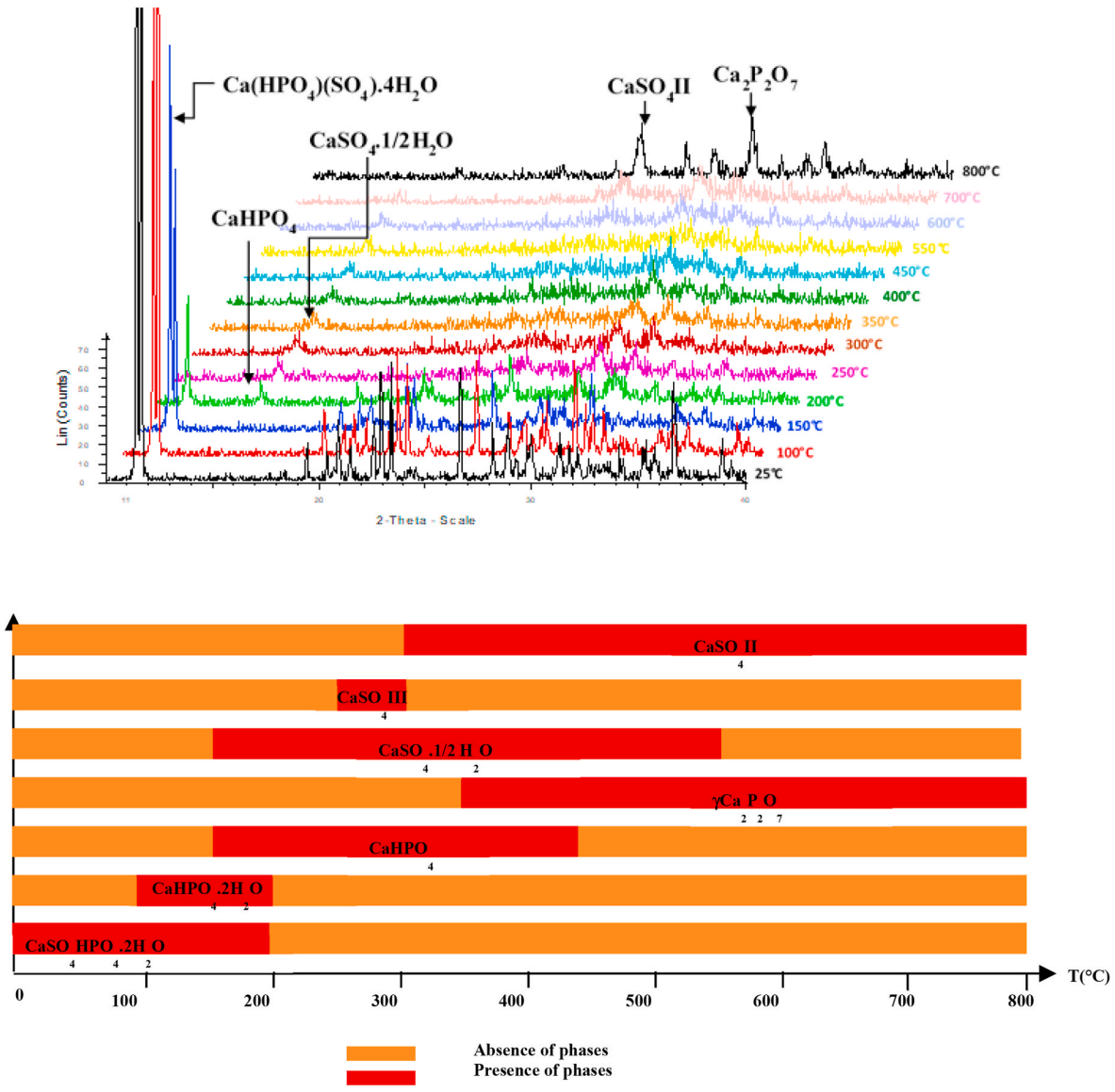

Fig. 12. A series of powder X-ray diffraction patterns taken during the calcination of ardealite.

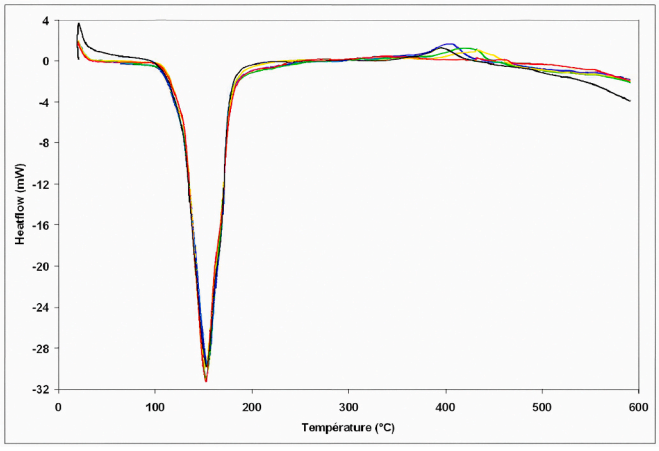

Fig. 13. Thermogravimetric curves of the solid solution with % HPO_4^{2-} = 0.25%, 0.5%, 0.8%, 1.5%.

The driving force of the hydration of the hemihydrate is the difference between its solubility and that of gypsum. The dissolution of the hemihydrate leads to a solution with a much higher ion concentration than gypsum under the same conditions. The hemihydrate solution is supersaturated with respect to the gypsum solution, and its degree of supersaturation is defined as follows:

$$\alpha = \frac{C}{C_s} \tag{14}$$

where C is the concentration of the hemihydrate solution and C_s is the saturation concentration of the gypsum solution. Indeed, the hemihydrate hydration solution undergoes variations in Ca^{2+} and SO_4^{2-} ion concentrations, which can be monitored by measuring the conductivity of the suspension. The dissolution of plaster is extremely rapid. The solution concentration reaches the apparent solubility of the hemihydrate as found in the study of Amathieu and Boistelle (1988). This concentration value corresponds to a competition between the dissolution rates of the hemihydrate on one hand, and the crystallization of gypsum on the other, and does not represent a thermodynamic equilibrium. The dissolution process follows second-order kinetics with respect to the concentrations. As reported in the research performed by

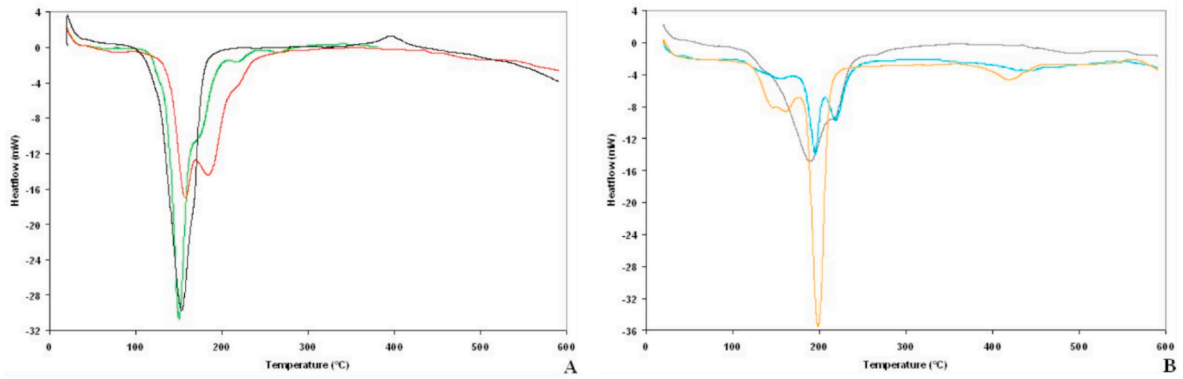

Fig. 14. Thermogravimetric curves of synthetic gypsums with 0% < HPO_4^{2-} < 100%. $CaSO_4{\cdot}2H_2O$, % HPO_4^{2-} = 5%, 30% (Fig. A); % HPO_4^{2-} = 40%, 80%, $CaHPO_4{\cdot}2H_2O$ (Fig. B).

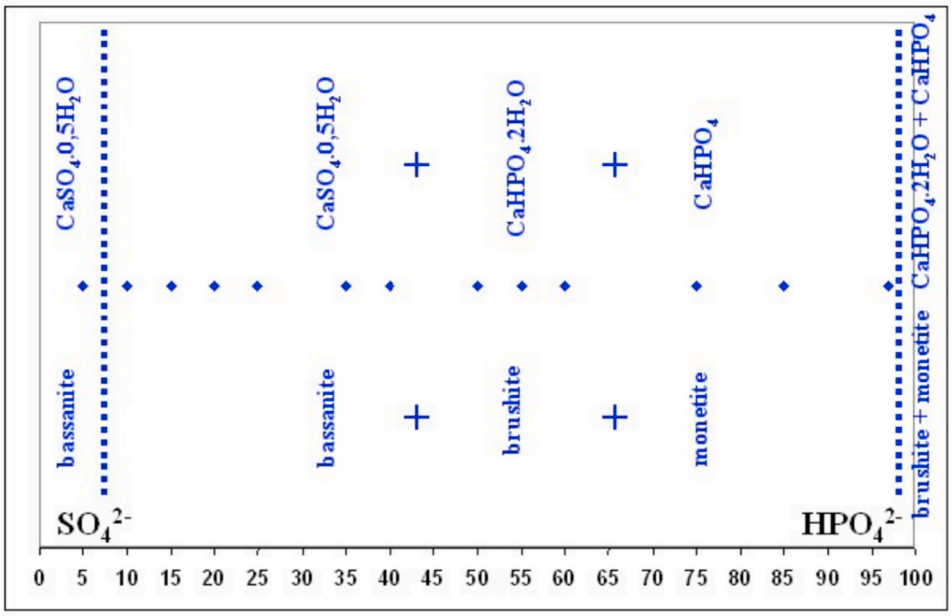

Fig. 15. Phases present in the $CaSO_4{\cdot}2H_2O$–$CaHPO_4{\cdot}2H_2O$ system at 150 °C determined by X-ray diffraction (XRD).

Amathieu and Boistelle (1988), the crystallization of gypsum commences, evidenced by the initial decrease in concentration. This process involves heterogeneous nucleation, however, homogeneous nuclei are anticipated to emerge only after 2–3 min, corresponding to the peak supersaturation ($\beta = \frac{K_{HH}}{Kgypsum}$ with $K_{HH} = 1.25 \times 10^{-4}$ $(mol/L)^2$). For about 3 min, the concentration of Ca^{2+} (or SO_4^{2-}) remains constant, suggesting a steady state in solution (latent period). This assumption is, however, inaccurate as the concentration of Ca^{2+} ions immediately decreases in solution, indicating the appearance of gypsum from the beginning (gypsum nucleation). The amount of gypsum formed remains low, about 5–10% of the precipitable mass. The solution is only slightly undersaturated compared to the hemihydrate, which therefore dissolves practically insignificantly during this phase. Then, a decrease in the concentrations of Ca^{2+} and SO_4^{2-} in solution initiates. Gypsum crystallization and growth already exist at this stage. The quantity of gypsum increases very rapidly. Between 5 and 15 min, the rapid decrease in conductivity indicates rapid growth of gypsum crystals, possibly still accompanied by nucleation phenomena near the initial plateau. The crystallization rate reaches a maximum of around 10 min and 30 s, the inflection point of the curve, at which there is no longer hemihydrate in suspension. Consequently, the solution is no longer supplied with sulfate and calcium ions. Since the solution concentrations decrease very quickly between 5 and 10 min and 30 s, this indicates that the dissolution rate of the hemihydrate is no longer sufficient to completely compensate for the crystallization kinetics of gypsum. The hydration process is completed after 15–20 min, leading to the terminal plateau of the conductometric curve, which reflects the solubility equilibrium of gypsum.

Brushite (0.31 g/L) is 10 times less soluble than hemihydrate (3.2 g/L). In water, brushite tends to undergo hydrolysis. The process of hydrolysis has been studied and dissected by Lerch et al. (1966). It involves several successive and parallel reactions:

Rapid and partial dispersion of the phosphate in water:

$$CaHPO_4{\cdot}2H_2O \leftrightarrow Ca^{2+} + HPO_4^{2-} \quad (15)$$

Rapid hydrolysis of hydrogen phosphate ions (HPO_4^{2-}):

$$HPO_4^{2-} + H_2O \leftrightarrow H_2PO_4^- + OH^- \quad (16)$$

Slow and concurrent dismutation reaction:

$$2HPO_4^{2-} \leftrightarrow PO_4^{3-} + H_2PO_4^- \quad (17)$$

$$2HPO_4^{2-} + H_2O \leftrightarrow 2\,H_2PO_4^- + 2OH^- \quad (18)$$

Precipitation of phosphate ions (PO_4^{3-}):

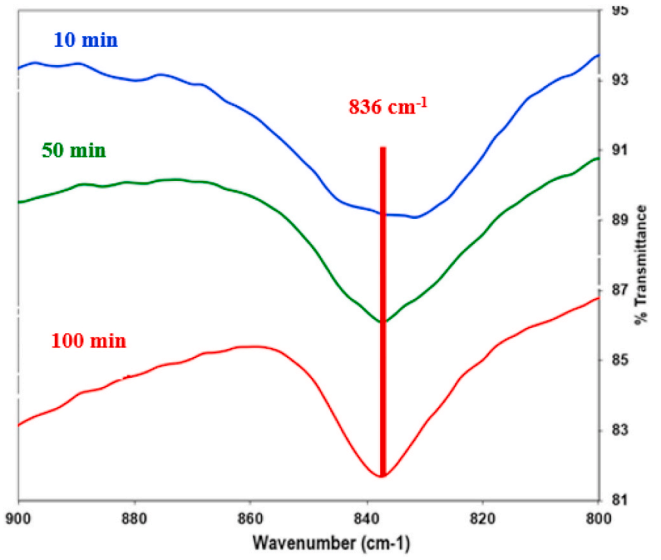

Fig. 16. IR absorption spectra of a solid solution as a function of calcining time at 150 °C.

$$PO_4^{3-} + Ca^{2+} + HPO_4^{2-} + OH^- \leftrightarrow \text{Calcium phosphate apatitic} \quad (19)$$

The calcium apatitic phosphate that precipitates is octocalcium phosphate. Overall, the hydrolysis reaction can be summarized as follows:

$$10CaHPO_4{\cdot}2H_2O \leftrightarrow Ca_8H_2(PO_4)_6{\cdot}5H_2O + 2Ca(H_2PO_4)_2{\cdot}H_2O \quad (20)$$

In the solution, monocalcium monohydrate phosphate appears, causing a decrease in pH. This phosphate is acidic. Its dissolution in water is incongruent and leaves behind H_3PO_4 as well as a residue of either $CaHPO_4{\cdot}2H_2O$ or $CaHPO_4$, according to Brown and Lehr. (1959).

Dihydrated calcium phosphate achieves optimal stability at pH 5.5, with hydrolysis becoming increasingly sensitive as pH rises. Regarding the kinetics, the dissolution of dicalcium phosphate dihydrate is slow and follows a first-order equation, suggesting a diffusion-controlled reaction, according to Djabri (1985). The solubilities of brushite and the products resulting from its dehydration vary (Fig. 17).

Lang Dupont (1985) conducted studies on the hydration of monetite and concluded that regardless of the sample's mass and the temperature at which the rehydration of $CaHPO_4$ occurs, the amount of water fixed after drying is consistently at a maximum of about 9% for finely pulverized samples. The experiment can be repeated multiple times on the same product, with the same amount of water being removed and fixed each time, which can be considered zeolitic. Only free water is susceptible to being fixed by anhydrous calcium phosphate.

5.1. Hydration of calcined solid solutions containing HPO_4^{2-} ions

During the synthesis of the solid solutions, the washing step was particularly important. The mineral acids and associated salts (notably KCl, K_2SO_4 and NaCl) accelerate the dissolution of the hemihydrate.As for the thermodynamic aspect, we consider the introduction of 1.5 g of a solid solution with a W/P ratio of 20 into 30 ml of distilled water. This solid solution consists of Ca^{2+}, $(1-y_i)SO_4^{2-}$, and $y_iHPO_4^{2-}$ was introduced. This process assumes that each component of the initial product undergoes congruent dissolution, eventually reprecipitating as a solid solution with the final composition: Ca^{2+}, $(1-y_f)SO_4^{2-}$, and $y_f\,HPO_4^{2-}$. In reality, this involves a series of precipitation and redissolution steps. Concentrations in the liquid phase and quantities of Ca^{2+}, SO_4^{2-} and HPO_4^{2-} in solid solution are calculated using the following relationships (we consider moles as the only conservative measure in our case, where there is an exchange of molecules between two phases):

1. Equilibria in the liquid solution: Phosphoric acid H_3PO_4 dissociates in solution. Applying the law of mass action to the dissociation equilibria of the three acidities yields the dissociation constants:

$$H_3PO_4 \leftrightarrow H^+ + H_2PO_4^- \quad K_1 = \frac{N(H^+)N(H_2PO_4^-)}{N(H_3PO_4)} \quad (21)$$

$$H_2PO_4^- \leftrightarrow H^+ + HPO_4^{2-} \quad K_2 = \frac{N(H^*)N(HPO_4{}^{2-})}{N(H_2PO_4^-)} \quad (22)$$

$$HPO_4{}^{2-} \leftrightarrow H^+ + PO_4{}^{3-} \quad K_3 = \frac{N(H^*)N(PO_4{}^{3-})}{N(HPO_4{}^{2-})} \quad (23)$$

With $K_1 = 10^{-2.16}$, $K_2 = 10^{-7.21}$ and $K_3 = 10^{-12.32}$

Four distinct forms can be distinguished based on the degree of dissociation: H_3PO_4, $H_2PO_4^-$, HPO_4^{2-}, and PO_4^{3-} (Fig. 18).

2. Equilibria in the solid phase: We express the conservation of sites in the solid, which is equivalent to stating the electroneutrality of the solid phase:

$$N_{Ca^{2+}\,sol.sol.} = N_{HPO_4{}^{2-}\,sol.sol.} + N_{SO_4{}^{2-}\,sol.sol.} \quad (24)$$

This equation applies to both the initial solid and the final solid.

3. Interphase Equilibria:

$$Ca^{2+}{}_{\text{sol. liq.}} + HPO_4^{2-}{}_{\text{sol. liq.}} = Ca^{2+}_{\text{sol. sol. G}} + HPO_4^{2-}{}_{\text{sol. sol. G}} \quad (25)$$

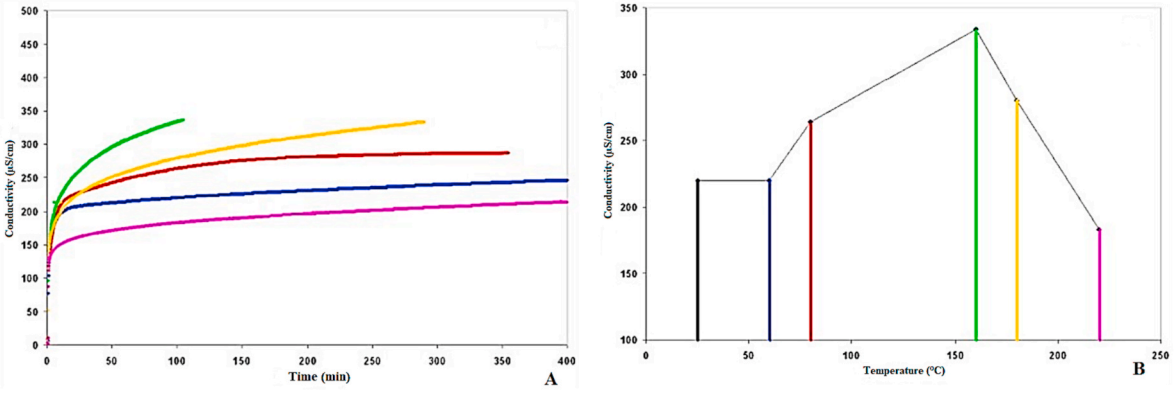

Fig. 17. Conductimetric curves (W/Brushite = 100) of calcined brushite samples at different temperatures (Fig. A). Conductivity at 100 min as a function of temperature (Fig. B). Brushite at 25 °C, T = 60 °C (these two curves overlap), T = 80 °C, T = 160 °C, T = 180 °C, and T = 220 °C.

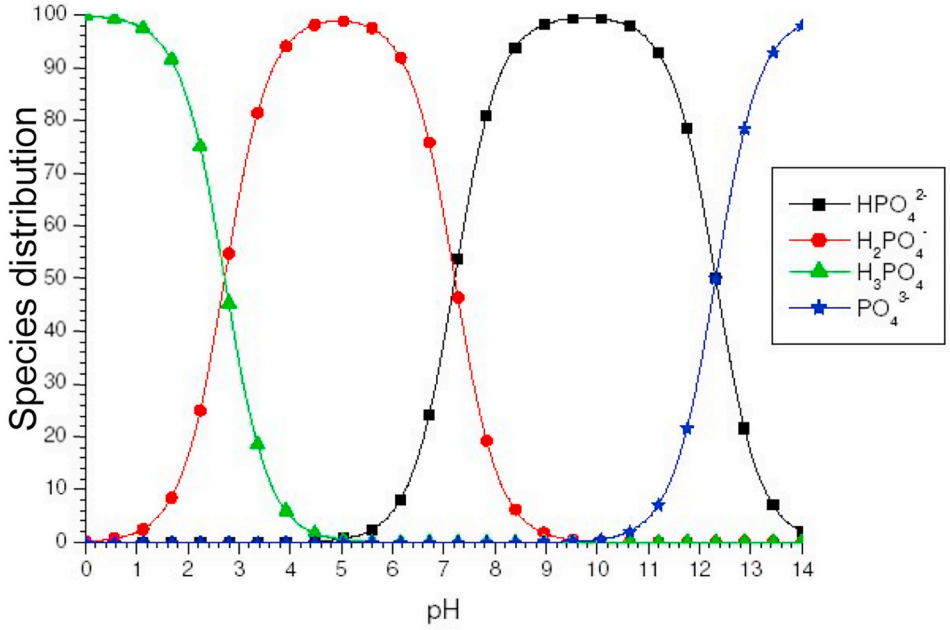

Fig. 18. Stability diagram of various forms of phosphoric acid.

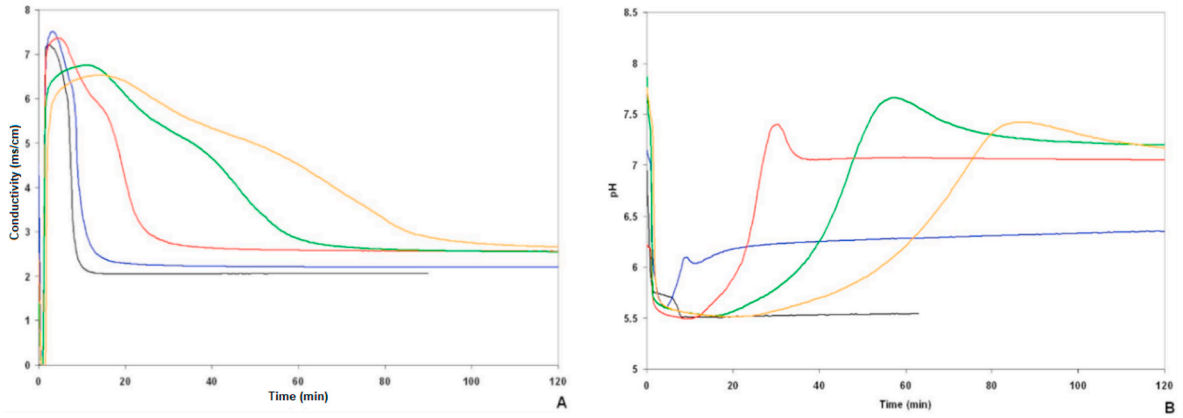

Fig. 19. Conductimetric (A) and pH-meter (B) curves of solid solution samples containing HPO_4^{2-} ions calcined at 150 °C (% HPO_4^{2-} = 0, 0.25%, 1.5%, 4% and 5%).

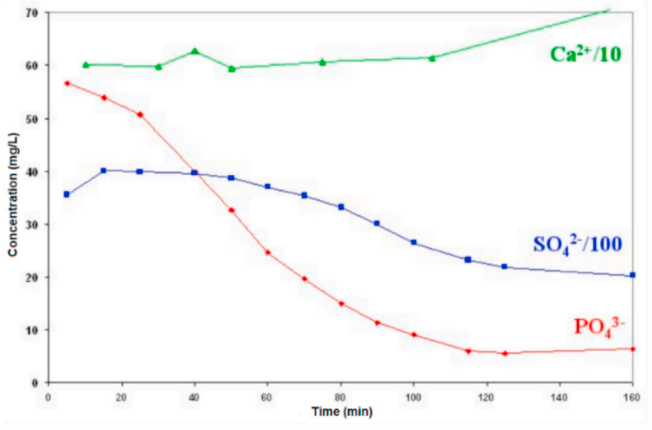

Fig. 20. Content of phosphates, sulfates/100 and calcium/10 of the samples taken during the hydration of a solid solution calcined at 150 °C and containing 5% of HPO_4^{2-}

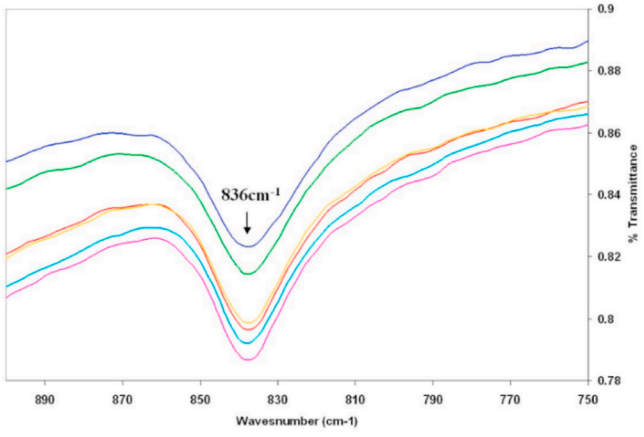

Fig. 21. IR spectra of samples taken during the hydration of a solid solution containing 5% of HPO_4^{2-} calcined at 150 °C (Time intervals: t = 5min, t = 25min, t = 60min, t = 90min, t = 125min, t = 160min).

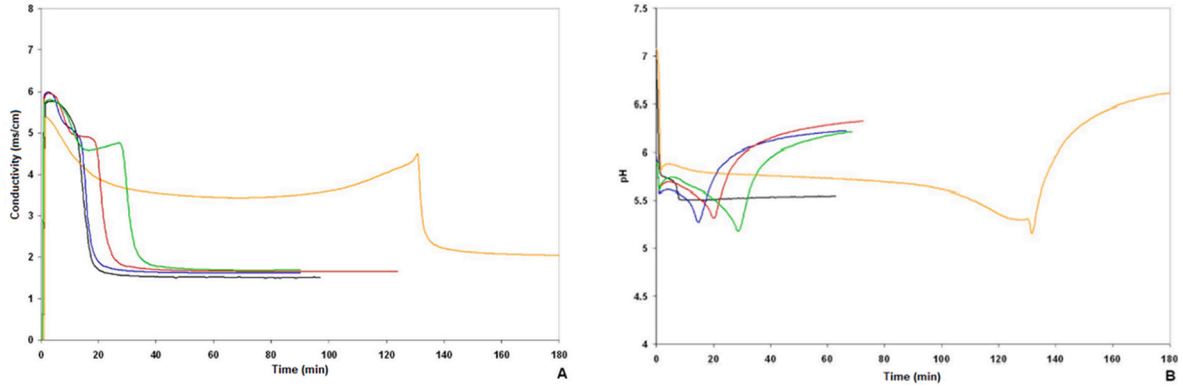

Fig. 22. Conductimetric (A) and pH-meter (B) curves of samples containing hemihydrate and brushite (% HPO_4^{2-} = 0.5%, 0.8%, 1.2%, 5%).

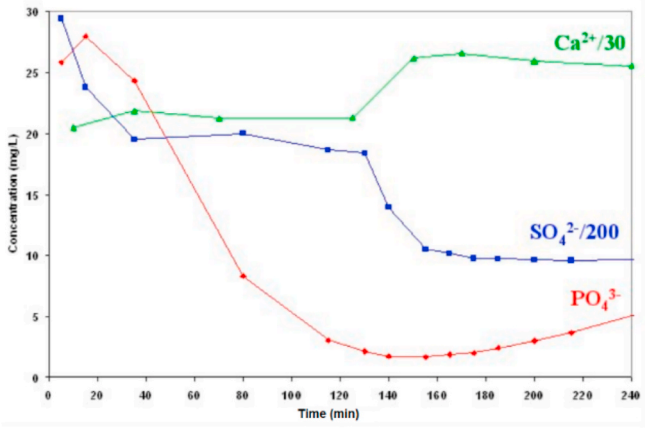

Fig. 23. Phosphate, sulfate/200, and calcium/30 contents of the samples collected during the hydration of a mixture of calcined hemihydrate and 5% brushite at 150 °C.

$$K_{x_1} = \frac{x_{Ca^{2+}\,sol.sol.G} \cdot x_{HPO_4^{2-}\,sol.sol.G}}{x_{Ca^{2+}\,sol.liq.} \cdot x_{HPO_4^{2-}\,sol.liq}} \quad (26)$$

$$Ca^{2+}_{\text{ sol. liq.}} + SO_4^{2-}{}_{\text{ sol. liq.}} = Ca^{2+}_{\text{sol. sol. G}} + SO_4^{2-}{}_{\text{ sol. sol. G}} \quad (27)$$

$$K_{x_2} = \frac{x_{Ca^{2+}\,sol.sol.G} \cdot x_{SO_4^{2-}\,sol.sol.G}}{x_{Ca^{2+}\,sol.liq.} \cdot x_{SO_4^{2-}\,sol.liq}} \quad (28)$$

$$K_p = \text{The partition coefficient} = \frac{x_{Ca^{2+}\,sol.sol.G} \cdot x_{HPO_4^{2-}\,sol.sol.G}}{x_{Ca^{2+}\,sol.sol.B} \cdot x_{HPO_4^{2-}\,sol.sol.B}} \quad (29)$$

Alternatively:

$$K_{SG} = x_{Ca^{2+}\,sol.liq.} \cdot x_{SO_4^{2-}\,sol.liq.} \quad (30)$$

$$K_{SB} = x_{Ca^{2+}\,sol.liq.} \cdot x_{HPO_4^{2-}\,sol.liq.} \quad (31)$$

And:

$$x_{Ca^{2+}\,sol.liq.} \approx \frac{N_{Ca^{2+}\,sol.sol.}}{N_{H^2O}} = \frac{N_{Ca^{2+}\,sol.sol.} \cdot V_M}{V_E} \approx C_{Ca^{2+}\,sol.liq.} \cdot V_M \quad (32)$$

Similarly:

$$x_{SO_4^{2-}\,sol.liq.} = C_{SO_4^{2-}\,sol.liq.} \cdot V_M \quad (33)$$

$$x_{HPO_4^{2-}\,sol.liq.} = x_{HPO_4^{2-}\,sol.liq.} \cdot V_M \quad (34)$$

$$K_{X2} = \frac{0,5 \cdot 0,5}{N_{SG} \cdot V_M{}^2} \cdot Kp \quad (35)$$

$$K_{X1} = \frac{0,5 \cdot 0,5}{N_{SB} \cdot V_M{}^2} \cdot Kp \quad (36)$$

4. Equations of species conservation:

$$N_{SO_4^{2-}\,sol.sol.f} + N_{SO_4^{2-}\,sol.liq.} = N_{SO_4^{2-}\,sol.sol.i} \quad (37)$$

$$N_{Ca^{2+}\,sol.sol.f} + N_{Ca^{2+}\,sol.liq.} = N_{Ca^{2+}\,sol.sol.i} \quad (38)$$

$$N_{H_3PO_4\,sol.liq.} + N_{H_2PO_4^-\,sol.liq.} + N_{HPO_4^{2-}\,sol.liq.} + N_{PO_4^{3-}\,sol.liq.} + N_{HPO_4^{2-}\,sol.sol.f} = N_{HPO_4^{2-}\,sol.sol.i} \quad (39)$$

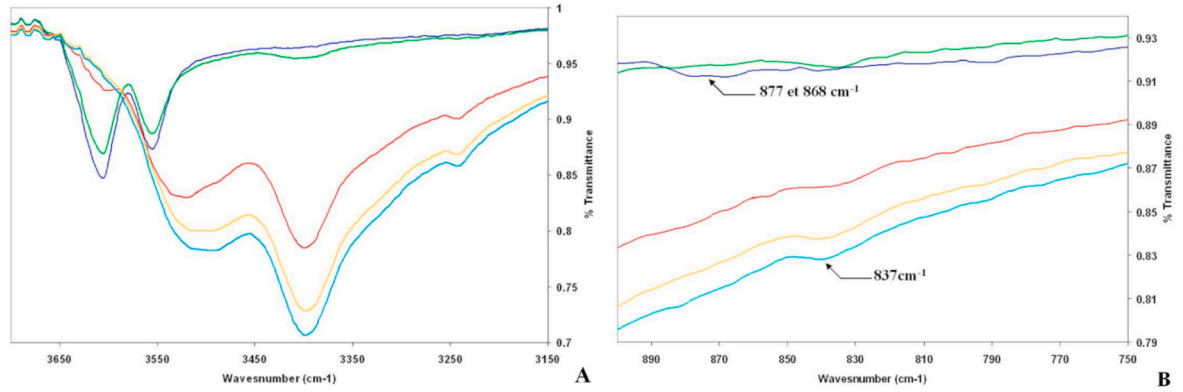

Fig. 24. IR Spectra of samples collected during the hydration of a mixture consisting of 95% gypsum and 5% brushite calcined at 150 °C (Time intervals: t = 5min, t = 15min, t = 80min, t = 130min, and t = 215min).

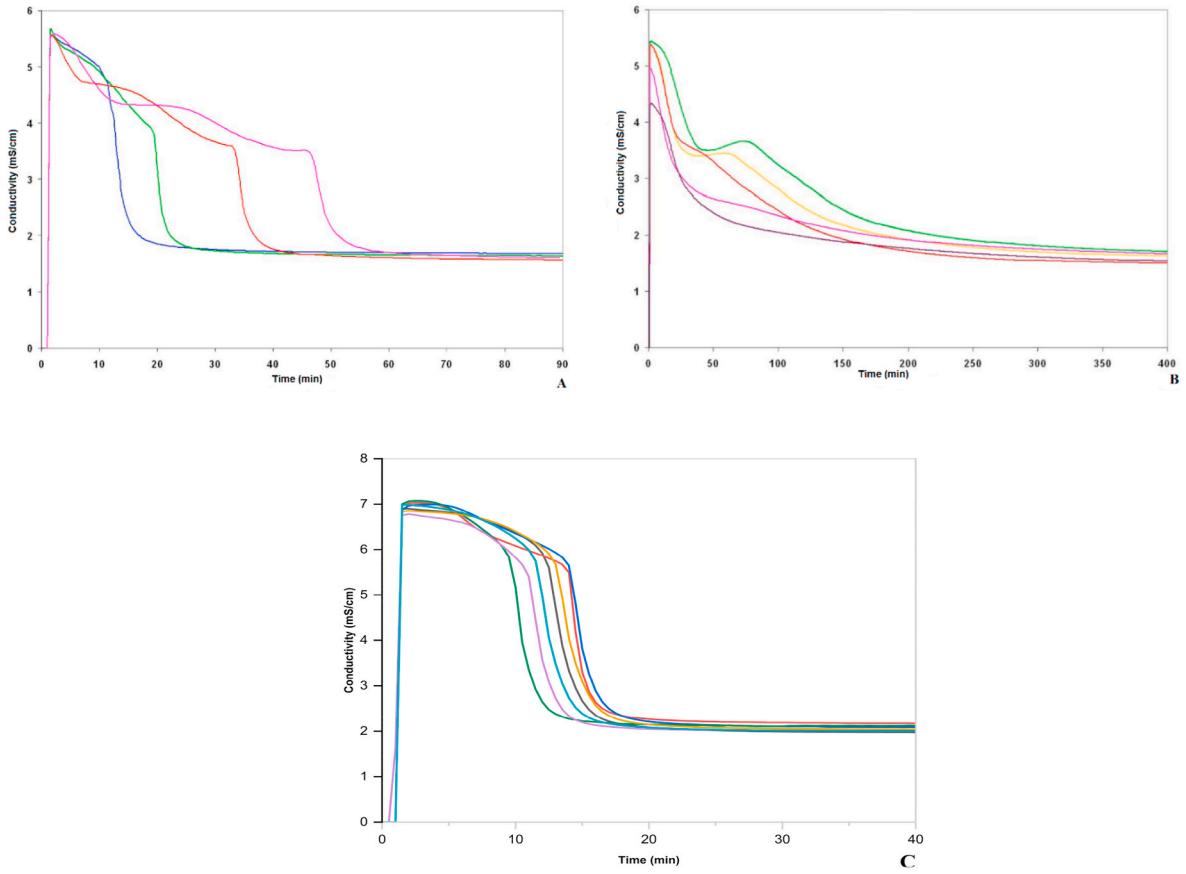

Fig. 25. Conductimetric curves of samples containing a mixture of 98% hemihydrate and 2% calcined brushite at different temperatures: Non-calcined, T = 60 °C, T = 100 °C, and T = 140 °C (A); T = 160 °C, T = 180 °C, T = 200 °C, T = 220 °C and T = 260 °C (B); T = 150 °C, T = 300 °C, T = 400 °C, T = 450 °C, T = 500 °C, T = 550 °C, T = 600 °C (C).

5. Electroneutrality of the liquid solution:

$$N_{H^+{}_{sol.liq.}} + 2N_{Ca^{2+}{}_{sol.liq.}} = N_{OH^-{}_{sol.liq.}} + 2N_{SO_4{}^{2-}{}_{sol.liq.}} + N_{H_2PO_4{}^-{}_{sol.liq.}} + 2N_{HPO_4{}^{2-}{}_{sol.liq.}} + 3N_{PO_4{}^{3-}{}_{sol.liq.}} \quad (40)$$

The variables are:

$$N_{Ca^{2+}{}_{sol.sol.f}}, N_{SO_4{}^{2-}{}_{sol.sol.f.}}, N_{HPO_4{}^{2-}{}_{sol.sol.f}}, N_{Ca^{2+}{}_{sol.liq.}}, N_{SO_4{}^{2-}{}_{sol.liq.}}, N_{H_3PO_4{}_{sol.liq.}}, N_{HPO_4{}^{2-}{}_{sol.liq.}}, N_{H_2PO_4{}^-{}_{sol.liq.}}, N_{PO_4{}^{3-}{}_{sol.liq.}}, N_{OH^-{}_{sol.liq.}}, N_{H^+{}_{sol.liq.}}$$

We have developed a system consisting of 11 equations, wherein each unknown variable is expressed in terms of the number of moles of H^+ ions in the liquid solution. This system is then solved numerically. As a result, we can determine various properties, such as the final pH of the liquid solution, based on the initial composition of the solid solution as outlined by Guilhot et al. (1974).

However, it should be noted that the system of equations, devised by Guilhot et al. (1974), does not incorporate the presence of the ardealite phase, which acts as an intermediary between gypsum and brushite. The simulations were conducted using a partition coefficient of 2.27, denoted as Kp = $\frac{17}{7.5}$, where the range $0.075 < x_{HPO_4{}^{2-}} < 0.17$ corresponds to the demixing zone between gypsum and brushite.

Regarding the kinetics aspect, the results of the hydration process reveal that the existence of syncrystallized HPO_4^{2-} within the hemihydrate significantly affects the duration necessary for the setting process. Notably, the setting time is prolonged as the concentration of syncrystallized HPO_4^{2-} increases. As illustrated in Fig. 19A, setting times range from 13 min for the lowest concentrations to 85 min for the highest concentrations, indicating that higher concentrations of HPO_4^{2-} ions result in longer setting times.

To elucidate these aforementioned phenomena, we conducted sampling at various time intervals for the sample containing 5% of HPO_4^{2-}. The samples were filtered, and the liquid phase was analyzed using ion chromatography, while the solid phase was characterized using IR spectroscopy. The shape of the curve relative to the concentration of sulfate ions in the liquid phase resembles that of the conductimetric curve (Fig. 19A and 20).

The absorption band characteristic of syncrystallized HPO_4^{2-} ions is consistently visible in all spectra, regardless of the sampling time (Fig. 21). These analyses confirm the occurrence of a sequential process involving dissolution and precipitation of a solid solution containing HPO_4^{2-} ions. Furthermore, for samples collected at 5 and 15 min, there is a slight bulge observed at 872 cm^{-1}. We had previously observed this absorption band in brushite, but it appears slightly shifted towards shorter wavelengths for samples with P/S ≥ 4.

The dissolution of the Ca^{2+}, SO_4^{2-}, and syncrystallized HPO_4^{2-} ions occurred simultaneously, indicating congruent dissolution. Initially, the

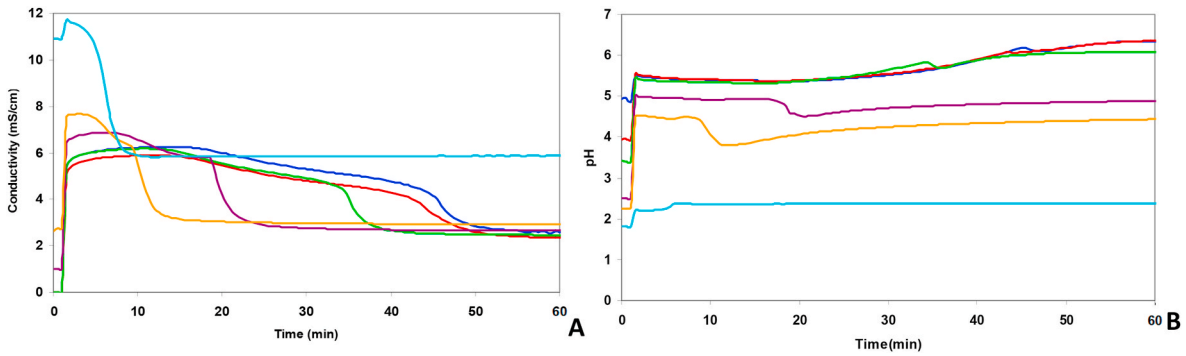

Fig. 26. Conductimetric curves (A) and pH meter curves (B) monitoring hydration in mixing water at acid pH of a calcined solid solution at 150 °C containing 5% of HPO_4^{2-} (pH = 5, pH = 4, pH = 3.5, pH = 2.5, pH = 2.3, pH = 1.9).

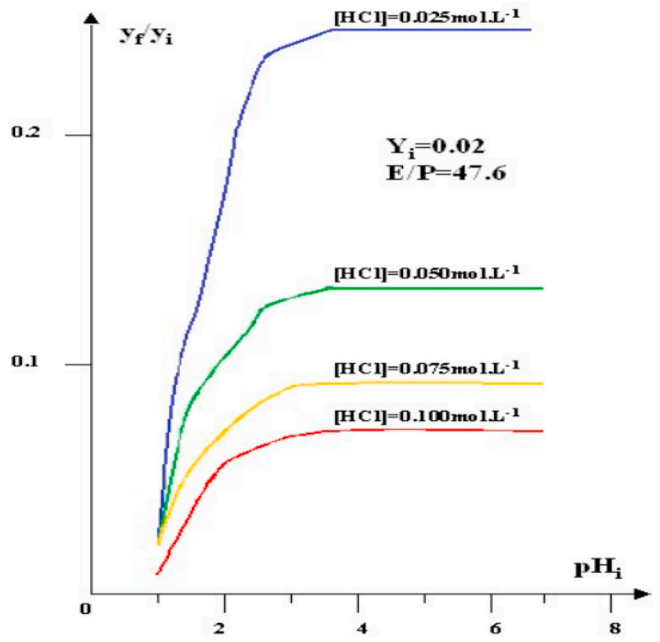

Fig. 27. Influence of hydrochloric acid addition on the equilibrium composition of the solid solution, theoretical curves according to analysis presented by Guilhot et al. (1974).

hemihydrate came into contact with water (pH = 7). At this pH (Fig. 19B), a portion of the syncrystallized HPO_4^{2-} ions transformed into $H_2PO_4^-$ ions by consuming H^+ ions from the solution (Fig. 18), according to the reaction:

$$HPO_4^{2-} + H^+ \rightarrow H_2PO_4^- \quad (41)$$

During this stage of hydration, the pH increased because the highly soluble $Ca(H_2PO_4)_2{\cdot}H_2O$ (18.3 g/L) did not precipitate. As the pH increased, the equilibrium between $H_2PO_4^-/HPO_4^{2-}$ shifted towards HPO_4^{2-}. The $CaHPO_4{\cdot}2H_2O$ phase, which is poorly soluble (0.31 g/L), became present in sufficient quantity to precipitate. During the precipitation, it carried away slightly excess SO_4^{2-} ions from the solution. Hence, brushite with syncrystallized SO_4^{2-} ions also precipitated. The absorption band located at 870 cm^{-1} indicated the presence of these phases. The loss of HPO_4^{2-} ions that occurred in the liquid phase led to an increase in the concentration of H^+ ions, resulting in a pH decrease.

As the hydration progressed, the solubility limit of calcium sulfate saturated with syncrystallized HPO_4^{2-} ions was reached, leading to the precipitation of the first crystals of this phase. The pH increased as the SO_4^{2-} ions were replaced by HPO_4^{2-} ions in the solution, thereby lowering the H^+/SO_4^{2-} ratio. Consequently, the gypsum phase with syncrystallized HPO_4^{2-} ions precipitated, carrying the residual HPO_4^{2-} ions along. This sequence of reactions led to an increase in the H^+ ion content of the solution and a subsequent decrease in pH.

At the end of the hydration process, there are three distinct coexisting phases: solid phases comprising gypsum with syncrystallized HPO_4^{2-} ions and brushite with syncrystallized SO_4^{2-} ions, alongside a liquid phase containing Ca^{2+}, SO_4^{2-}, HPO_4^{2-}, $H_2PO_4^-$, H^+, and OH^- ions. These three phases are not in equilibrium; therefore, relatively slow dissolution and recrystallization phenomena occur. This is due to the fact that gypsum and brushite phases are less soluble compared to the initial hemihydrate. The composition of the final product differed from that of the initial product since some ions, such as SO_4^{2-} and HPO_4^{2-}, remained in the solution.

Furthermore, in Fig. 19A, we observe that as the initial content of syncrystallized HPO_4^{2-} ions increases, the duration during which the gypsum saturated in HPO_4^{2-} and brushite saturated in HPO_4^{2-} precipitate simultaneously also increases. This is not surprising because the quantity of each precipitating phase increases.

The syncrystallized HPO_4^{2-} ions in the hemihydrate are responsible for the delay in setting, and we now understand the mechanism behind this delay. However, we seek to understand the role these HPO_4^{2-} ions play when they are in the brushite and/or monetite phases.

5.2. Hydration of hemihydrate-brushite mixture

A mixture of gypsum and brushite was calcined at 150 °C under a nitrogen atmosphere for 5 h. At this calcination temperature, the brushite was transformed into a mixture containing 74% brushite and 26% monetite, displaying properties different from those of pure brushite and monetite.

The increase in the content of brushite calcined to 150 °C led to an increase in the setting time, as shown in Fig. 22A. It is observed that the germination process was blocked, indicating a delay in the formation of crystals. The shape of the pH-meter curves is singular (Fig. 22B).

To investigate these phenomena, we carried out sampling at different times for samples containing 5% HPO_4^{2-}. These specimens were filtered, and the liquid phase was analyzed using ion chromatography (Fig. 23), while the solid phase was analyzed using infrared spectrometry.The shape of the curve regarding the concentration of sulfate ions in the liquid phase is similar to the conductometric curve (Figs. 23 and 22A). The IR spectra reveal the presence of hemihydrate for the samples collected at 5 and 15 min, as evidenced by the characteristic water absorption bands at 3555 and 3604 cm^{-1} (Fig. 24). Additionally, for the sample collected at 5 min, the absorption band at 870 cm^{-1} indicates the presence of brushite. All other spectra exhibit an absorption band at 837 cm^{-1}, indicating the existence of syncrystallized HPO_4^{2-} ions within the gypsum.

By analyzing the pH meter curve of the sample, it can be observed that initially, the hemihydrate dissolved, resulting in a decrease in pH

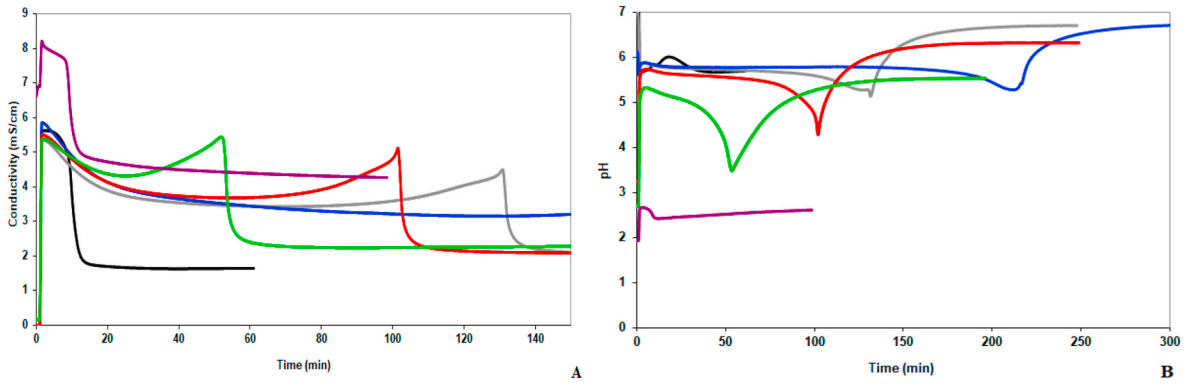

Fig. 28. Conductimetric curves (A) and pH meter curves (B) monitoring hydration in mixing water at acid pH of a mixture comprising 95% gypsum and 5% brushite calcined at 150 °C (pH(100% hemihydrate) = 7, pH = 7, pH = 3, pH = 2.7, pH = 2).

values. Subsequently, HPO_4^{2-} ions began to be released from brushite (0.31 g/L) and monetite (0.3 g/L) phases, whose solubility is quite similar. These ions transform HPO_4^{2-} ions by consuming H^+ ions, leading to a subsequent rise in pH.

As the process progresses, the gypsum phase precipitates along with HPO_4^{2-} ions, causing a subsequent decline in pH. Notably, brushite with syncrystallized SO_4^{2-} ions do not precipitate due to the faster dissolution rate of hemihydrate compared to brushite and monetite. Additionally, the solubility limit of the gypsum phase with HPO_4^{2-} ions is quickly reached.

The pH continues to increase as the solid system becomes saturated with HPO_4^{2-} ions, which are then released into the solution. The presence of HPO_4^{2-} ions from the brushite calcined at 150 °C (with 74% monetite and 26% brushite) significantly contributes to a delay in setting.

The study also investigated the reactivity of a mixture comprising 98% hemihydrate and 2% calcined brushite at different temperatures. Notably, the setting time reaches its maximum for hydration of this mixture at 160 °C (Fig. 25). It is important to note that at this temperature, the monetite begins to crystallize. As monetite is inert, it does not react with water. Consequently, as the temperature rises, brushite gradually transforms into monetite until it is completely transformed. This phenomenon explains the decrease in setting time observed up to 160 °C (Fig. 25 B and C). Furthermore, for brushite calcination temperatures above 280 °C, where only monetite is present as shown in the dehydration section, the conductimetric curves coincide with those of the hemihydrate without any additives (Fig. 25C). It can be concluded that the calcination temperature of brushite, and consequently the proportion of brushite and monetite present, has a direct influence on the reactivity of the plaster it is composed of.

5.3. Influence of pH on the hydration of the obtained products

The effect of the initial pH of the liquid solution on these systems was also investigated, which included a solid solution containing HPO_4^{2-} ions and a mixture of gypsum and brushite calcined at 150 °C. The pH of the mixing water was modified using HCl.

Reducing the pH of the mixing water leads to a notable decrease in the setting time of the mixture (Fig. 26). This is attributed to the shift in equilibrium towards the formation of HPO_4^{2-} ions and phosphoric acid (Fig. 18). The mechanism is identical to that described above. However, the sharp rise in pH observed at the start of hydration corresponds to a reaction that consumes H^+ ions:

$$2HPO_4^{2-} + 2H^+ \rightarrow H_2PO_4^- + H_3PO_4 \quad (42)$$

The resolution of the equation system presented in the paragraph dealing with the hydration of calcined solid solutions with HPO_4^{2-} has shown that it is possible to significantly reduce the content of syncrystallized HPO_4^{2-} ions in the final product by lowering the initial pH of the aqueous solution used to hydrate the hemihydrate. The addition of even a small amount of HCl can have a considerable effect on this content, as shown in Fig. 26. This aspect has not previously been investigated experimentally. The experimental results obtained with hydrochloric acid are consistent with the predictions of the mathematical model, as shown in Fig. 27.

It should be noted that the shape of the curves remains consistent whatever the pH. The only variation is in germination, which decreases with decreasing pH (Fig. 28). It can be concluded that under acidic pH conditions, the setting time decreases.

In summary, the calcination process conducted at 150 °C induces a transformation of gypsum-based products into hemihydrate. The study of their hydration revealed that HPO_4^{2-} ions significantly delayed the setting time when they were in syncrystallized form, especially when originating from the brushite phase calcined at 150 °C. To address this issue, adjusting the calcination temperature emerges as a promising solution. Industries may find it advantageous to opt for lower temperatures when processing phosphogypsum with such impurities. Additionally, we have identified pH adjustments in the mixing water as an effective means of accelerating the setting time.

6. Conclusion

Our research focuses on addressing challenges associated with impurities, particularly syncrystallized phosphates HPO_4^{2-} ions, in the context of utilizing phosphogypsum as a building material. These ions can substitute for SO_4^{2-} ions in gypsum to form solid solutions, and their presence can be quantified using IR spectroscopy. The maximum amount of HPO_4^{2-} ions that can enter the gypsum lattice is 10%, leading to crystallizing sand rose rather than acicular or needle crystals. As the content of HPO_4^{2-} ions increases, a new phase appears: ardealite $Ca(SO_4)_{1-x}(PO_4)_x.2H_2O$ with $0.42 < x < 0.54$, followed by brushite: $CaHPO_4.2H_2O$.

Our investigation has extended to studying the dehydration behaviors of both pure phases and solid solutions. We have observed that the presence of syncrystallized HPO_4^{2-} ions leads to a higher transformation temperature from anhydrite III to anhydrite II compared to pure gypsum. Furthermore, during the calcination of brushite at 150 °C, we have noticed that there is neither complete dehydration nor transition through a subhydrated phase, but rather the formation of a mixture of two phases: brushite, and monetite, which exhibit different properties compared to their pure counterparts.

The reactivity of our samples, in the form of plaster, was assessed using various techniques including conductometry, pH-meter readings, solution sampling, and analysis of residual solids during hydration. Our research has revealed that hemihydrate compounds containing HPO_4^{2-} ions, derived from the dehydration of brushite forming a mixture of

brushite and monetite, exhibit a notable delay in hydration. This delay is especially pronounced at a calcination temperature of 160 °C, where monetite begins to crystallize. Monetite, being inert, does not react with water. As the temperature increases, brushite gradually transform into monetite until complete transition occurs. This phenomenon explains the observed decrease in setting times up to 160 °C.

In light of these findings, brushite calcined at 160 °C emerges as the most detrimental impurity. However, adjusting the calcination temperature, whether lowering or raising it, has shown potential in mitigating the delaying effect on hydration. Hence, from an industrial standpoint, it is advisable to calcine PG containing this impurity at the lowest feasible temperature. Moreover, we have discovered that lowering the pH of the mixing water can effectively accelerate the setting time. These insights shed light on the complexities surrounding impurities in PG and offer valuable guidance for optimizing its utilization in the plaster industry.

CRediT authorship contribution statement

Hajar Bellefqih: Conceptualization, Formal analysis, Investigation, Methodology, Writing – original draft, Writing – review & editing. **Véronique Bourgier:** Formal analysis, Methodology, Writing – review & editing. **Essaid Bilal:** Conceptualization, Data curation, Formal analysis, Funding acquisition, Investigation, Methodology, Project administration, Resources, Supervision, Writing – review & editing. **Delia-Georgeta Dumitraş:** Formal analysis, Investigation, Methodology, Writing – review & editing. **Ştefan Marincea:** Conceptualization, Formal analysis, Investigation, Methodology, Writing – review & editing. **Hamid Mazouz:** Conceptualization, Formal analysis, Funding acquisition, Investigation, Methodology, Project administration, Writing – review & editing. **Nils Haneklaus:** Formal analysis, Funding acquisition, Project administration, Writing – review & editing.

Declaration of competing interest

The authors declare that they have no known competing financial interests or personal relationships that could have appeared to influence the work reported in this paper.

Data availability

Data will be made available on request.

Acknowledgement

French National Research Agency (ANR) and German Federal Ministry of Education and Research (Project Number: 033RU020A) support for this project is offered under the coordination of the ERA-MIN3 action, which has received funding from the European Union under the Horizon 2020 Program (European Commission Grant Agreement No. 101003575). This work was further supported by the Federal Ministry of Education, Science and Research (BMBWF) through Austria's Agency for Education and Internationalization (OeAD) [Grant Number: FR 12/2024]. Supplementary funds were obtained through the PN 23-39-02-06 and PN 23-39-02-07 projects, funded by the Ministry of Research, Innovation and Digitalization in Romania.

References

Abbona Christensson, M., Franchini Angela C, F.F., Lundager Madsen, H., 1993. Crystal habit and growth conditions of brushite, $CaHPO_4 \cdot 2H_2O$. J. Cryst. Growth 131, 331–346. https://doi.org/10.1016/0022-0248(93)90183-W.

Abdelhadi, N.A., Abdelhadi, M.A., El-Hasan, T.M., 2014. The characteristics of cement mortars utilizes the untreated phosphogypsum wastes generated from fertilizer plant, Aqaba-Jordan. Jordan J. Earth Environ. Sci. 6.

Akfas, F., Elghali, A., Aboulaich, A., Munoz, M., Benzaazoua, M., Bodinier, J.L., 2024. Exploring the potential reuse of phosphogypsum: a waste or a resource? Sci. Total Environ. 168196 https://doi.org/10.1016/j.scitotenv.2023.168196.

Allevi, S., Marchi, M., Scotti, F., Bertini, S., Cosentino, C., 2016. Hydration of calcium sulphoaluminate clinker with additions of different calcium sulphate sources. Mater. Struct. 49, 453–466.

Altun, İ.A., Sert, Y., 2004. Utilization of weathered phosphogypsum as set retarder in Portland cement. Cement Concr. Res. 34, 677–680. https://doi.org/10.1016/j.cemconres.2003.10.017.

Amathieu, L., Boistelle, R., 1988. Crystallization kinetics of gypsum from dense suspension of hemihydrate in water. J. Cryst. Growth 88, 183–192.

Anbalagan, G., Mukundakumari, S., Murugesan, K.S., Gunasekaran, S., 2009. Infrared, optical absorption, and EPR spectroscopic studies on natural gypsum. Vib. Spectrosc. 50, 226–230. https://doi.org/10.1016/j.vibspec.2008.12.004.

Arifuzzaman, S.M., Rohani, S., 2004. Experimental study of brushite precipitation. J. Cryst. Growth 267, 624–634. https://doi.org/10.1016/j.jcrysgro.2004.04.024.

Aslanian, S., Stoilova, D., Petrova, R., 1980. Isodimorphe Substitution im $CaSO_4$-$CaHPO_4$-H_2O System. Z. Anorg. Allg. Chem. 465, 209–220. https://doi.org/10.1002/zaac.19804650125.

Bagade, M.A., Satone, S.R., 2012. An experimental investigation of partial replacement of cement by various percentage of Phosphogypsum in cement concrete. Int. J. Eng. Res. Afr. 2248–9622.

Becker, P., others, 1989. Phosphates and Phosphoric Acid: Raw Materials, Technology, and Economics of the Wet Process. Revised and Expanded. Marcel Dekker, Inc.

Bian, X., Zeng, L., Ji, F., Xie, M., Hong, Z., 2022. Plasticity role in strength behavior of cement-phosphogypsum stabilized soils. J. Rock Mech. Geotech. Eng. 14, 1977–1988. https://doi.org/10.1016/j.jrmge.2022.01.003.

Bilal, E., Bellefqih, H., Bourgier, V., Mazouz, H., Dumitraş, D.-G., Bard, F., Laborde, M., Caspar, J.P., Guilhot, B., Iatan, L., Bounakhla, M., Iancu, M.A., Marincea, Ş., Essakhraoui, M., Li, B., Diwa, R.R., Ramirez, J.D., Chernysh, Y., Chubur, V., Roubík, H., Schmidt, H., Beniazza, R., Cánovas, C.R., Nieto, J.M., Haneklaus, N., 2023. Phosphogypsum circular economy considerations: a critical review from more than 65 storage sites worldwide. J. Clean. Prod. 137561 https://doi.org/10.1016/j.jclepro.2023.137561.

Brown, W.E., Lehr, J.R., 1959. Application of phase rule to the chemical behavior of monocalcium phosphate monohydrate in soils. Soil Sci. Soc. Am. J. 23, 7–12.

Burnett, W.C., Schultz, M.K., Hull, C.D., 1996. Radionuclide flow during the conversion of phosphogypsum to ammonium sulfate. J. Environ. Radioact. 32, 33–51. https://doi.org/10.1016/0265-931X(95)00078-O.

Cai, Q., Jiang, J., Ma, B., Shao, Z., Hu, Y., Qian, B., Wang, L., 2021. Efficient removal of phosphate impurities in waste phosphogypsum for the production of cement. Sci. Total Environ. 780, 146600 https://doi.org/10.1016/j.scitotenv.2021.146600.

Cánovas, C.R., Chapron, S., Arrachart, G., Pellet-Rostaing, S., 2019. Leaching of rare earth elements (REEs) and impurities from phosphogypsum: a preliminary insight for further recovery of critical raw materials. J. Clean. Prod. 219, 225–235. https://doi.org/10.1016/j.jclepro.2019.02.104.

Chen, X., Gao, J., Zhao, Y., 2019. Investigation on the hydration of hemihydrate phosphogypsum after post treatment. Construct. Build. Mater. 229 https://doi.org/10.1016/j.conbuildmat.2019.116864.

Chernysh, Y., Yakhnenko, O., Chubur, V., Roubík, H., 2021. Phosphogypsum recycling: a review of environmental issues, current trends, and prospects. Appl. Sci. 11, 1–22. https://doi.org/10.3390/app11041575.

Costa, R.P., de Medeiros, M.H.G., Rodriguez Martinez, E.D., Quarcioni, V.A., Suzuki, S., Kirchheim, A.P., 2022. Effect of soluble phosphate, fluoride, and pH in Brazilian phosphogypsum used as setting retarder on Portland cement hydration. Case Stud. Constr. Mater. 17 https://doi.org/10.1016/j.cscm.2022.e01413.

Degirmenci, N., Okucu, A., Turabi, A., 2007. Application of phosphogypsum in soil stabilization. Build. Environ. 42, 3393–3398. https://doi.org/10.1016/j.buildenv.2006.08.010.

Djabri, Z., 1985. Rôle du gypse dans l'insolubilisation des orthophosphates : étude physicochimique des mécanismes mis en jeu.

Dosen, A., Giese, R.F., 2011. Thermal decomposition of brushite, $CaHPO_4 \cdot 2H_2O$ to monetite $CaHPO_4$ and the formation of an amorphous phase. Am. Mineral. 96 (2–3), 368–373. https://doi.org/10.2138/am.2011.3544.

Dumitraş, D.-G., 2017. A re-investigation of ardealite from the type locality, the "dry" Cioclovina Cave (Şureanu Mountains, Romania). Eur. J. Mineral 29 (6), 1055–1066. https://doi.org/10.1127/ejm/2017/0029-2655.

Dumitras, D.-G., Marincea, S., Fransolet, A.-M., 2004. Brushite in the bat guano deposit from the "dry" Cioclovina cave (Sureanu Mountains, Romania). Neues Jahrb. fur Mineral. Abh 180, 45–64. https://doi.org/10.1127/0077-7757/2004/0180-0045.

Engbrecht, D.C., Hirschfeld, D.A., 2016. Thermal analysis of calcium sulfate dihydrate sources used to manufacture gypsum wallboard. Thermochim. Acta 639, 173–185. https://doi.org/10.1016/j.tca.2016.07.021.

Ennaciri, Y., Bettach, M., 2018. Procedure to convert phosphogypsum waste into valuable products. Mater. Manuf. Process. 33, 1727–1733.

Ennaciri, Y., Bettach, M., 2023. The chemical behavior of the different impurities present in Phosphogypsum: a review. Phosphorus, Sulfur, Silicon Relat. Elem. 1–20.

Ennaciri, Y., Zdah, I., El Alaoui-Belghiti, H., Bettach, M., 2020. Characterization and purification of waste phosphogypsum to make it suitable for use in the plaster and the cement industry. Chem. Eng. Commun. 207, 382–392.

Frost, R.L., Palmer, S.J., 2011. Thermal stability of the "cave" mineral brushite $CaHPO_4 \cdot 2H_2O$ - mechanism of formation and decomposition. Thermochim. Acta 521, 14–17. https://doi.org/10.1016/j.tca.2011.03.035.

García-Maté, M., Angeles, G., León-Reina, L., Losilla, E.R., Aranda, M.A.G., Santacruz, I., 2015. Effect of calcium sulfate source on the hydration of calcium sulfoaluminate eco-cement. Cem. Concr. Compos. 55, 53–61.

Geraldo, R.H., Costa, A.R.D., Kanai, J., Silva, J.S., Souza, J.D., Andrade, H.M.C., Gonçalves, J.P., Fontanini, P.S.P., Camarini, G., 2020. Calcination parameters on

phosphogypsum waste recycling. Construct. Build. Mater. 256 https://doi.org/10.1016/j.conbuildmat.2020.119406.
Grabas, K., Pawełczyk, A., Stręk, W., Szełęg, E., Stręk, S., 2019. Study on the properties of waste apatite phosphogypsum as a raw material of prospective applications. Waste Biomass Valori 10, 3143–3155. https://doi.org/10.1007/s12649-018-0316-8.
Gu, K., Chen, B., Pan, Y., 2020. Utilization of untreated-phosphogypsum as filling and binding material in preparing grouting materials. Construct. Build. Mater. 265 https://doi.org/10.1016/j.conbuildmat.2020.120749.
Guilhot, B., Gardet, M., Soustelle, Caspar, J., 1974. Etude des impuretés en solution solide dans le gypse : Cas des phosphogypses. Rapport interne confidentiel Ecole Nationale Supérieure des Mines de Saint-Etienne - Lafarge.
Hakkar, M., Arhouni, F.E., Mahrou, A., Bilal, E., Bertau, M., Roy, A., Steiner, G., Haneklaus, N., Mazouz, H., Boukhair, A., Benjelloun, M., 2021. Enhancing rare earth element transfer from phosphate rock to phosphoric acid using an inexpensive fly ash additive. Miner. Eng. 172, 107166 https://doi.org/10.1016/j.mineng.2021.107166.
Haneklaus, N., Barbossa, S., Basallote, M.D., Bertau, M., Bilal, E., Chajduk, E., Chernysh, Y., Chubur, V., Cruz, J., Dziarczykowski, K., Fröhlich, P., Grosseau, P., Mazouz, H., Kiegiel, K., Nieto, J.M., Pavón, S., Pessanha, S., Pryzowicz, A., Roubík, H., Cánovas, C.R., Schmidt, H., Seeling, R., Zakrzewska-Kołtuniewicz, G., 2022. Closing the upcoming EU gypsum gap with phosphogypsum. Resour. Conserv. Recycl. 182 https://doi.org/10.1016/j.resconrec.2022.106328.
Huang, Y., Lin, Z., 2011. A binder of phosphogypsum-ground granulated blast furnace slag-ordinary portland cement. J. Wuhan Univ. Technol.-Materials Sci. Ed. 26, 548–551.
Jia, R., Wang, Q., Luo, T., 2021. Reuse of phosphogypsum as hemihydrate gypsum: the negative effect and content control of H3PO4. Resour. Conserv. Recycl. 174, 105830.
Jin, Z., Ma, B., Su, Y., Lu, W., Qi, H., Hu, P., 2020. Effect of calcium sulphoaluminate cement on mechanical strength and waterproof properties of beta-hemihydrate phosphogypsum. Construct. Build. Mater. 242 https://doi.org/10.1016/j.conbuildmat.2020.118198.
Jin, Z., Cui, C., Xu, Z., Lu, W., Su, Y., He, X., Chen, S., Li, W., Wang, B., 2023. Recycling of waste gypsum from αlpha-hemihydrate phosphogypsum: based on the atmospheric hydrothermal process. Construct. Build. Mater. 377 https://doi.org/10.1016/j.conbuildmat.2023.131136.
Klepetsanis, P.G., Koutsoukos, P.G., 1998. Kinetics of calcium sulfate formation in aqueous media: effect of organophosphorus compounds. Waste Biomass Valori. 193 (1–2), 156–163.
Kuzmanović, P., Todorović, N., Mrđa, D., Forkapić, S., Petrović, L.F., Miljević, B., Hansman, J., Knežević, J., 2021. The possibility of the phosphogypsum use in the production of brick: radiological and structural characterization. J. Hazard Mater. 413, 125343.
Lang Dupont, M., 1985. Contribution à l'étude du phosphate bicalcique hydraté. Université de Paris.
Lerch, P., Lemp, R., Krahenbu, U., Bosset, J., 1966. Etude de l'hydrolyse de l'orthophosphate dicalcique dihydrate. Chimia. 20, 430–432.
Liu, W., Zheng, J., Ou, X., Liu, X., Song, Y., Tian, C., Rong, W., Shi, Z., Dang, Z., Lin, Z., 2018. Effective extraction of Cr (VI) from hazardous gypsum sludge via controlling the phase transformation and chromium species. Environ. Sci. Technol. 52, 13336–13342.
Li, X., Zhang, Q., 2021. Dehydration behaviour and impurity change of phosphogypsum during calcination. Constr. Build. Mater. 311. https://doi.org/10.1016/j.conbuildmat.2021.125328.
Liu, S., Fang, P., Ren, J., Li, S., 2020. Application of lime neutralised phosphogypsum in supersulfated cement. J. Clean. Prod. 272 https://doi.org/10.1016/j.jclepro.2020.122660.
Ma, X., Yao, S., Yuan, Z., Bi, R., Wu, X., Zhang, J., Wang, S., Wang, X., Jia, Y., 2020. Detoxification and reclamation of hydrometallurgical arsenic-and trace metals-bearing gypsum via hydrothermal recrystallization in acid solution. Chemosphere 250, 126290.
Mahmoud, M.H.H., Rashad, M.M., Ibrahim, I.A., Abdel-Aal, E.A., 2004. Crystal modification of calcium sulfate dihydrate in the presence of some surface-active agents. J. Colloid Interface Sci. 270, 99–105. https://doi.org/10.1016/j.jcis.2003.09.023.
Mirwald, P.W., 2008. Experimental study of the dehydration reactions gypsum-bassanite and bassanite-anhydrite at high pressure: indication of anomalous behavior of H_2O at high pressure in the temperature range of 50-300°C. J. Chem. Phys. 128 (7) https://doi.org/10.1063/1.2826321.
Moalla, R., Gargouri, M., Khmiri, F., Kamoun, L., Zairi, M., 2018. Phosphogypsum purification for plaster production: a process optimization using full factorial design. Environ. Eng. Res. 23, 36–45.
Möschner, G., Lothenbach, B., Figi, R., Kretzschmar, R., 2009. Influence of citric acid on the hydration of Portland cement. Cement Concr. Res. 39, 275–282.
Ölmez, H., Erdem, E., 1989. The effects of phosphogypsum on the setting and mechanical properties of Portland cement and trass cement. Cement Concr. Res. 19, 377–384.
Onac, P., J, B., Fornos, J., Ginés, À., Ginés, J., 2005. Mineralogical reconnaissance of caves from mallorca island. Endins: publicació d'espeleologia. 131–140.
Oumnih, S., Bekkouch, N., Gharibi, E.K., Fagel, N., Elhamouti, K., El Ouahabi, M., 2019. Phosphogypsum waste as additives to lime stabilization of bentonite. Sustain. Environ. Res. 1 https://doi.org/10.1186/s42834-019-0038-z.
Peng, X., Zheng, J., Liu, Q., Hu, Q., Sun, X., Li, J., Liu, W., Lin, Z., 2021. Efficient removal of iron from red gypsum via synergistic regulation of gypsum phase transformation and iron speciation. Sci. Total Environ. 791, 148319.
Pinto, A.J., Carneiro, J., Katsikopoulos, D., Jiménez, A., Prieto, M., Velasco, A., 2011. The link between brushite and gypsum: miscibility, dehydration and crystallochemical behavior in the CaHPO4. 2H 2 O-CaSO 4. 2H 2 O system. Cryst. Growth Des. 12 (1), 445–455.
Płachciak, M., 2020. Numerical assessment of the radiological impact of dust inhalation from phosphogypsum piles. Thèse de maîtrise. Universitat Politècnica de Catalunya.
Potgieter, J.H., Potgieter, S.S., McCrindle, R.I., Strydom, C.A., 2003. An investigation into the effect of various chemical and physical treatments of a South African phosphogypsum to render it suitable as a set retarder for cement. Cement Concr. Res. 33, 1223–1227. https://doi.org/10.1016/S0008-8846(03)00036-X.
Qi, J., Zhu, H., Zhou, P., Wang, X., Wang, Z., Yang, S., Yang, D., Li, B., 2023. Application of phosphogypsum in soilization: a review. Int. J. Environ. Sci. Technol. 20, 10449–10464. https://doi.org/10.1007/s13762-023-04783-2.
Qin, X., Cao, Y., Guan, H., Hu, Q., Liu, Z., Xu, J., Hu, B., Zhang, Z., Luo, R., 2023a. Resource utilization and development of phosphogypsum-based materials in civil engineering. J. Clean. Prod. https://doi.org/10.1016/j.jclepro.2023.135858.
Qin, X., Cao, Y., Guan, H., Hu, Q., Liu, Z., Xu, J., Hu, B., Zhang, Z., Luo, R., 2023b. Resource utilization and development of phosphogypsum-based materials in civil engineering. J. Clean. Prod. 387, 135858.
Rashad, A.M., 2017. Phosphogypsum as a construction material. J. Clean. Prod. 166, 732–743.
Rinaudo, C., Lanfranco, A.M., Boistelle, R., 1996. The gypsum-brushite system: crystallization from solutions poisoned by phosphate ions. J. Cryst. Growth 158.
Roode-Gutzmer, Q., Strydom, C., 1999. The characterization of phosphogypsum and gypsum-brushite mixtures by X-ray diffraction, thermogravimetric and differential scanning calorimetric techniques. Concr. Sci. Eng 1 (1999), 222–227.
Rosales, J., Pérez, S.M., Cabrera, M., Gázquez, M.J., Bolivar, J.P., de Brito, J., Agrela, F., 2020. Treated phosphogypsum as an alternative set regulator and mineral addition in cement production. J. Clean. Prod. 244 https://doi.org/10.1016/j.jclepro.2019.118752.
Rutherford, P.M., Dudas, M.J., Arocena, J.M., 1996. Heterogeneous distribution of radionuclides, barium and strontium in phosphogypsum by-product. Sci. Total Environ. 180 (3), 201–209. https://doi.org/10.1016/0048-9697(95)04939-8.
Rychkov, V.N., Kirillov, E.V., Kirillov, S.V., Semenishchev, V.S., Bunkov, G.M., Botalov, M.S., Smyshlyaev, D.V., Malyshev, A.S., 2018. Recovery of rare earth elements from phosphogypsum. J. Clean. Prod. 196, 674–681. https://doi.org/10.1016/j.jclepro.2018.06.114.
Saadaoui, E., Ghazel, N., Ben Romdhane, C., Massoudi, N., 2017. Phosphogypsum: potential uses and problems–a review. Int. J. Environ. Sci. 74, 558–567. https://doi.org/10.1080/00207233.2017.1330582.
Shih, W.Y., Rahardianto, A., Lee, R.W., Cohen, Y., 2005. Morphometric characterization of calcium sulfate dihydrate (gypsum) scale on reverse osmosis membranes. J. Membr. Sci. 252, 253–263. https://doi.org/10.1016/j.memsci.2004.12.023.
Singh, M., 2002. Treating waste phosphogypsum for cement and plaster manufacture. Cement Concr. Res. 32 (7), 1033–1038.
Singh, M., 2003. Effect of phosphatic and fluoride impurities of phosphogypsum on the properties of selenite plaster. Cement Concr. Res. 33, 1363–1369. https://doi.org/10.1016/S0008-8846(03)00068-1.
Singh, M., 2005. Role of phosphogypsum impurities on strength and microstructure of selenite plaster. Construct. Build. Mater. 19, 480–486. https://doi.org/10.1016/j.conbuildmat.2004.07.010.
Singh, M., Garg, M., Rehsi, S.S., 1993. Purifying phosphogypsum for cement manufacture. Construct. Build. Mater. 7, 3–7.
Singh, M., Garg, M., Verma, C.L., Handa, S.K., Kumar, R., 1996. An improved process for the purification of phosphogypsum. Construct. Build. Mater. 10, 597–600.
Taher, M.A., 2007. Influence of thermally treated phosphogypsum on the properties of Portland slag cement. Resour. Conserv. Recycl. 52, 28–38.
Tayibi, H., Choura, M., López, F.A., Alguacil, F.J., López-Delgado, A., 2009. Environmental impact and management of phosphogypsum. J. Environ. Manag. https://doi.org/10.1016/j.jenvman.2009.03.007.
Toshima, T., Hamai, R., Tafu, M., Takemura, Y., Fujita, S., Chohji, T., Tanda, S., Li, S., Qin, G.W., 2014. Morphology control of brushite prepared by aqueous solution synthesis. J. Asian Ceram. Soc. 2, 52–56. https://doi.org/10.1016/j.jascer.2014.01.004.
Walawalkar, M., Nichol, C.K., Azimi, G., 2016. Process investigation of the acid leaching of rare earth elements from phosphogypsum using HCl, HNO_3, and H_2SO_4. Hydrometallurgy 166, 195–204. https://doi.org/10.1016/j.hydromet.2016.06.008.
Winnefeld, F., Lothenbach, B., 2010. Hydration of calcium sulfoaluminate cements—experimental findings and thermodynamic modelling. Cement Concr. Res. 40, 1239–1247.
Zhou, S., Li, X., Zhou, Y., Min, C., Shi, Y., 2020. Effect of phosphorus on the properties of phosphogypsum-based cemented backfill. J. Hazard Mater. 399, 122993.